6692 *Chem. Mater.* **2010,** *22,* 6692–6710
DOI:10.1021/cm102891d

CHEMISTRY OF MATERIALS
Article

Multifunctional Polyurea Aerogels from Isocyanates and Water. A Structure−Property Case Study

Nicholas Leventis,*[,†] Chariklia Sotiriou-Leventis,*[,†] Naveen Chandrasekaran,[†] Sudhir Mulik,[†] Zachary J. Larimore,[‡] Hongbing Lu,*[,§] Gitogo Churu,[§] and Joseph T. Mang*[,∥]

[†]*Department of Chemistry, Missouri University of Science and Technology, Rolla, Missouri 65409, United States ,* [‡]*Department of Mechanical Engineering, Missouri University of Science and Technology, Rolla, Missouri 65409, United States ,* [§]*Department of Mechanical Engineering, University of Texas at Dallas, Richardson, Texas 75080, United States , and* [∥] *Los Alamos National Laboratory, Los Alamos, New Mexico 87545, United States*

Received October 7, 2010

It is well-known that isocyanates and water yield polyureas; however, that reaction is not generally associated with the synthesis of the latter, being used instead for environmental curing of films baring free NCO groups or for foaming polyurethanes. Here we report that careful control of the relative isocyanate/water/catalyst (Et_3N) ratio in acetone, acetonitrile, or DMSO prevents precipitation, yielding instead polyurea (PUA) gels convertible to highly porous (up to 98.6% v/v) aerogels over a very wide density range (0.016−0.55 g cm^{-3}). The method has been implemented successfully with several aliphatic and aromatic di and triisocyanates. PUA aerogels have been studied at the molecular level (^{13}C NMR, IR, XRD), the elementary nanoparticle level (SANS/USANS), and the microscopic level (SEM). Their porous structure has been probed with N_2-sorption porosimetry. Despite that the nanomorphology varies with density from fibrous at the low density end to particulate at the high density end, all samples consist of similarly sized primary particles assembled differently, probably via a reaction-limited cluster−cluster aggregation mechanism at the low density end, which changes into diffusion-limited aggregation as the isocyanate concentration increases. Higher density PUA aerogels (>0.3 g cm^{-3}) are mechanically strong enough to tolerate the capillary forces of evaporating low surface tension solvents (e.g., pentane) and can be dried under ambient pressure; under compression, they can absorb energy (up to 90 J g^{-1} at 0.55 g cm^{-3}) at levels observed only with polyurea-cross-linked silica and vanadia aerogels (50−190 J g^{-1} at similar densities). At cryogenic temperatures (−173 °C) PUA aerogels remain relatively ductile, a fact attributed to sintering effects and their entangled fibrous nanomorphology. Upon pyrolysis (> 500 °C, Ar), PUA aerogels from aromatic isocyanates are converted to carbon aerogels in high yields (∼60% w/w). Those properties, considered together with the simple synthetic protocol, render PUA aerogels attractive multifunctional materials.

1. Introduction

Quasi-stable, low-density, three-dimensional assemblies of nanoparticles are referred to as aerogels and typically are derived from drying wet-gels by turning the pore-filling solvent into a supercritical fluid (SCF).[1] Their large internal void space is responsible for very low thermal conductivities and high acoustic attenuation. The combination of those properties is extremely attractive for practical applications. There are two types of aerogels, organic and inorganic. They were first reported together by S. Kistler in 1931, noting that certain organic aerogels (e.g., those of nitrocellulose) were more robust materials than their inorganic counterparts.[2] However, emphasis of early research on the latter created a momentum that left purely organic aerogels dormant for almost 60 years, until the late 1980s, when R. Pekala started reporting his systematic studies on aerogels based on resorcinol−formaldehyde (RF) phenolic-type resins.[3] Phenolic (phenol−formaldehyde) resins were already in use since the late 1950s for the preparation of glassy (vitreous) carbon.[4] Thus, the impetus of Pekala's work and almost all subsequent efforts on phenolic aerogels was their conversion to high surface area electrically conducting carbon aerogels.[5] Nevertheless, the record-low thermal conductivity of RF aerogels

(1) Pierre, A. C.; Pajonk, G. M. *Chem. Rev.* **2002**, *102*, 4243–4265.
(2) (a) Kistler, S. S. *Nature* **1931**, *127*, 3211. (b) Kistler, S. S. *J. Phys. Chem.* **1932**, *36*, 52–63.
(3) (a) Pekala, R. K. Low Density, Resorcinol-Formaldehyde Aerogels. U.S. Patent No. 4,873,218, 1989. (b) Pekala, R. W. *J. Mater. Sci.* **1989**, *24*, 3221–3227. (c) Pekala, R. W.; Alviso, C. T.; Kong, F. M.; Hulsey, S. S. *J. Non-Cryst. Solids* **1992**, *145*, 90–98. (d) Pekala, R. W.; Schaefer, D. W. *Macromolecules* **1993**, *26*, 5887–5893.
(4) (a) Redfern, B. Bodies and Shapes of Carbonaceous Materials and Processes for their Production. U.S. Patent No. 3,109,712, 1963. (b) Cowlard, F. C.; Lewis, J. C. *J. Mater. Sci.* **1967**, *2*, 507–512.
(5) (a) Mayer, S. T.; Pekala, R. W.; Kaschmitter, J. L. *J. Electrochem. Soc.* **1993**, *140*, 446–451. (b) Ritter, J. A.; Al-Muhtaseb, S. A. *Adv. Mater.* **2003**, *15*, 101–114.

Published on Web 12/03/2010

(0.012 W m^{-1} K^{-1} at 0.16 g cm^{-3}) was noticed early,[6] creating interest for a closer look and further development in the broader area of organic aerogels.

Part of that interest was due to the fact that applications of inorganic aerogels, and in particular those based on silica, were stumbling across fragility problems. Those issues have been addressed successfully by post-gelation casting of a thin conformal polymer coating over the entire internal porous surface of the preformed wet-gel nanostructure.[7] The coating connects chemically the skeletal nanoparticles and provides the interparticle necks with the extra chemical energy of the interparticle polymeric tethers. Thus, the internal void space is not compromised significantly, while the flexural strength of a typical monolith is increased by a factor of over 300× for a nominal increase in density by a factor of 3. This process is referred to as cross-linking and the resulting aerogels as polymer-cross-linked aerogels (X-aerogels). New applications for aerogels, as in ballistic protection, are within reach.[8]

The cross-linking process was recently extended to RF aerogels to render them more robust. Thus, dangling hydroxyl groups on the surface of the RF skeletal nanoparticles (RF−OH) were connected via reaction with Desmodur N3300A, a trifunctional isocyanate supplied by Bayer (see below).[9] The polyurea aerogels described herewith were the result of a curious observation along that process: when the cross-linking reaction of the triisocyanate with the RF−OH groups was assisted (catalyzed) with a base (triethylamine, Et_3N), the triisocyanate bathing solution gelled, yielding a gel (RF) inside another, which clearly came from gelation of the isocyanate.

Direct gelation of isocyanates has been reported and studied since the 1950s as a side reaction during formation of polyurethanes. Specifically, it was noted that certain catalysts cause gelation of isocyanate-terminated polyurethane prepolymers by cross-linking polymeric chains through allophanate bridges, while others cause gelation through trimerization of the isocyanates into isocyanurates.[10] Without hard chemical evidence, the first purposeful conversion of a multifunctional isocyanate into polyisocyanurate aerogels was reported in the mid 1990s by De Vos and Biesmans;[11] the process used Suprasec DNR,[12] (a condensation oligomer of 4,4′-diphenylmethane diisocyanate, abbreviated as MDI) and several trimerization catalysts, most notably 1,4-diazobicyclo[2.2.2]octane (DABCO).[11] Those aerogels demonstrated exceptionally low thermal conductivities (8.5 and 15 W m^{-1} K^{-1} for evacuated (< 10 mbar) and air-filled 0.21 g cm^{-3} samples, respectively) and high surface areas (about 300 m^2 g^{-1} at 0.24 g cm^{-3}), and upon pyrolysis under inert atmosphere they yielded carbon aerogels with yields (∼40% w/w) comparable to those obtained from RF aerogels (∼50% w/w). However, the outer gel obtained during cross-linking of RF wet-gels was not the product of base-catalyzed trimerization of the isocyanate groups; that gel was found to consist of polyurea (abbreviated herewith as PUA) formed via the Et_3N-catalyzed reaction of the triisocyanate with residual water in the cross-linking bath.

In general, polyureas and polyurethanes are prepared from isocyanates and multifunctional amines or alcohols, respectively. High surface area polyurethanes as the stationary phase for chromatographic separations were reported in the early 1970s via reaction in CH_2Cl_2 of polymeric MDI (e.g., Mondur MR) and a pentafunctional oligomer made by oxypropylation of diethylenetriamine.[13] Those materials were first obtained as precipitates rather than gels; however, later modification of the process with more polar solvents and sugar derivatives as the polyols yielded gels and eventually aerogels. For example, Tan et al. used toluene diisocyanate to cross-link and induce pyridine-catalyzed gelation of acetone solutions of cellulose acetate and cellulose acetate butyrate. The resulting wet-gels were dried to aerogels with SCF CO_2. The motivation of that work was synthesis of high impact strength aerogels, although the mechanical properties were not quantified.[14] A similar approach was followed later by Rigacci et al. who, with an eye to thermal superinsulation, used a DABCO-catalyzed reaction of an MDI derivative with saccharose and pentaerythritol in DMSO/ethyl acetate mixtures.[15] The MDI derivative was Lupranat M20S by ICI, a product similar to Suprasec DNR (see above), and the result was nanoparticulate polyurethane aerogels, whose macro- versus mesoporosity was

(6) Lu, X.; Arduini-Schuster, M. C.; Kuhn, J.; Nilsson, O.; Fricke, J.; Pekala, R. W. *Science* **1992**, *255*, 971–972.
(7) (a) Leventis, N.; Sotiriou-Leventis, C.; Zhang, G.; Rawashdeh, A.-M. M. *Nano Lett*. **2002**, *2*, 957–960. (b) Zhang, G.; Dass, A.; Rawashdeh, A.-M. M.; Thomas, J.; Counsil, J. A.; Sotiriou-Leventis, C.; Fabrizio, E. F.; Ilhan, F.; Vassilaras, P.; Scheiman, D. A.; McCorkle, L.; Palczer, A.; Johnston, J. C.; Meador, M. A. B.; Leventis, N. *J. Non-Cryst. Solids* **2004**, *350*, 152–164. (c) Leventis, N.; Mulik, S.; Wang, X.; Dass, A.; Sotiriou-Leventis, C.; Lu, H. *J. Am. Chem. Soc*. **2007**, *129*, 10660–10661. (d) Leventis, N. *Acc. Chem. Res*. **2007**, *40*, 874–884. (e) Mulik, S.; Sotiriou-Leventis, C.; Churu, G.; Lu, H.; Leventis, N. *Chem. Mater*. **2008**, *20*, 5035–5046. (f) Leventis, N.; Mulik, S.; Wang, X.; Dass, A.; Patil, V. U.; Sotiriou-Leventis, C.; Lu, H.; Churu, G.; Capecelatro, A. *J. Non-Cryst. Solids* **2008**, *354*, 632–644. (g) Leventis, N.; Sotiriou-Leventis, C. Methods and Compositions for Preparing Silica Aerogels. U.S. Patent No. 7,771,609, 2010. (h) Eychmüller, A. *Angew. Chem., Int. Ed*. **2005**, *44*, 4839–4841.
(8) (a) Leventis, N.; Sotiriou-Leventis, C.; Mulik, S.; A. Dass, A.; Schnobrich, J.; Hobbs, A.; Fabrizio, E. F.; Luo, H.; Churu, G.; Zhang, Y.; Lu, H. *J. Mater. Chem*. **2008**, *18*, 2475–2482. (b) Luo, H.; Churu, G.; Schnobrich, J.; Hobbs, A.; Fabrizio, E. F.; Dass, A.; Mulik, S.; Sotiriou-Leventis, C.; Lu, H.; Leventis, N. *J. Sol-Gel Sci. Technol*. **2008**, *48*, 113–134.
(9) Leventis, N.; Mulik, S.; Sotiriou-Leventis, C. *Chem. Mater*. **2008**, *20*, 6985–6997.
(10) (a) Britain, J. W. *Ind. Eng. Chem. Prod. Res. Dev*. **1962**, *1*, 261–264. (b) Richter, F. U.; Schmitz, J.; Laas, H.-J.; Halpaap, R. *Polym. Prepr*. **2003**, *44*, 46–47.
(11) (a) De Vos R.; Biesmans, G. L. J. G. Organic Aerogels. U.S. Patent No. 5,484,818, 1994. (b) Biesmans, G.; Randall, D.; Francais, E.; Perrut, M. *J. Non-Cryst. Solids* **1998**, *225*, 36–40. (c) Biesmans, G.; Mertens, A.; Duffours, L.; Woignier, T.; Phalippou, J. *J. Non-Cryst. Solids* **1998**, *225*, 64–68. (d) Biesmans, G. L. J. G. Polyisocyanate Based Aerogels. U.S. Patent No. 5,990,184, 1999. (e) Biesmans, G. L.; Mertens, A. Organic Aerogels. U.S. Patent No. 5,942,553, 1999.
(12) *Resins for Coatings, Chemistry, Properties and Applications*; Stoye, D., Freitag, W., Eds.; Hanser/Gardner Publications, Inc.: Munich, 1996; p 186.
(13) (a) Ross, W. D.; Jefferson, R. T. *J. Chromatogr. Sci*. **1970**, *8*, 386–389. (b) Hileman, F. D.; Sievers, R. E.; Hess, G. G.; Ross, W. D. *Anal. Chem*. **1973**, *45*, 1126–1130.
(14) Tan, C.; Fung, B. M.; Newman, J. K.; Vu, C. *Adv. Mater*. **2001**, *13*, 644–646.
(15) Rigacci, A.; Marechal, J. C.; Repoux, M.; Moreno, M.; Achard, P. *J. Non-Cryst. Solids* **2004**, *350*, 372–378.

controlled by adjusting the Hildebrand solubility parameter via the DMSO/ethylacetate ratio. Reported thermal conductivities were lower than those of standard polyurethane foams (0.022 vs 0.030 W m^{-1} K^{-1}, respectively, at room temperature and atmospheric pressure and bulk densities, ρ_b, at ~0.2 g cm^{-3}).[15] Later, Fischer and Rigacci revisited the Tan et al. approach of cross-linking cellulose acetate in acetone using again Lupranat M20S and dibutyltin laurate as catalyst; those aerogels were considered "green," because they involved a natural product (cellulose) and demonstrated very high elastic moduli (in the 200−300 MPa range at $0.75 \leq \rho_b \leq 0.85$ g cm^{-3}) and low thermal conductivities ranging from 0.029 W m^{-1} K^{-1} (at atmospheric pressure) to 0.006 W m^{-1} K^{-1} (at 2×10^{-5} mbar) for samples with $\rho_b = 0.25$ g cm^{-3}.[16]

Polyurea (PUA) aerogels were first mentioned in the De Vos−Biesmans 1994 U.S. Patent,[11a] while a detailed comparative study with polyurethane and silica aerogels, mainly from a thermal insulation perspective, was published recently by Lee, Gould, and Rhine.[17] The latter were synthesized in acetone via Et_3N-catalyzed reaction of MDI, or polymeric MDI-type isocyanates with triamines, while polyurethane aerogels were prepared from the same isocyanates and an ethylene oxide-modified polyether polyol (Multranol 9185). PUA aerogels were nanoparticulate like silica while polyurethane aerogels were nanofibrous, similar to the materials reported by Fischer and Rigacci (see above).[16] At similar densities (0.12−0.13 g cm^{-3}) PUA aerogels demonstrated lower thermal conductivities than polyurethane aerogels (0.018−0.019 W m^{-1} K^{-1}, vs 0.027 W m^{-1} K^{-1}, respectively). Both aerogel types, however, had higher thermal conductivity values than 0.09 g cm^{-3} silica (0.012 W m^{-1} K^{-1}).

Polyureas are also the result of the reaction of isocyanates with water by a sequence that initially yields amines through decomposition of unstable carbamic acids (eq 1).

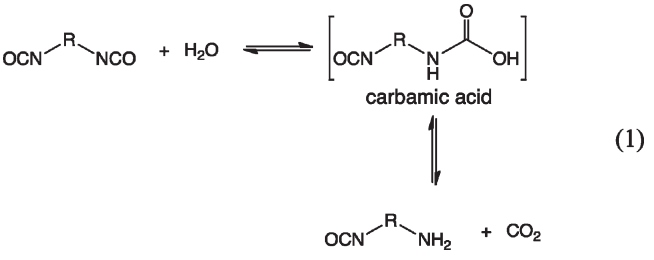

(1)

The amine product of eq 1 reacts further with yet-unreacted isocyanate yielding urea (eq 2).

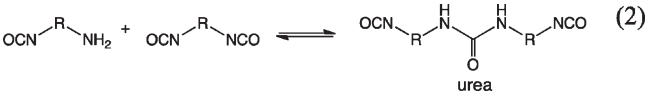

(2)

Reaction 2 takes place much faster than reaction 1, because amines are much better nucleophiles than water.[18]

However, the sequence of the reactions 1 and 2 is not associated with the typical synthetic methods of bulk polyureas. Instead, it is involved in the environmental curing of films baring free isocyanates, while, owing to the CO_2 side product, it is also used for the formation of polyurethane foams whereas a small amount of water added in the reaction mixture acts as a foaming agent.[19] That process though can be also very attractive from a materials synthesis perspective, because it replaces use of expensive amines with "green" water. As it will become evident below, from an aerogels perspective the method works best with triisocyanates such as Desmodur N3300A and Desmodur RE, yielding monoliths over a quite wide density range (0.016−0.55 g cm^{-3}). Diisocyanates such as Desmodur N3200, toluene diisocyanate (TDI), or monomeric MDI also gel, but only at higher concentrations. The ensuing discussion is based on aerogels derived from (a) Desmodur N3300A for their variable nanomorphology as a function of density and their mechanical properties, which are comparable, and in some aspects superior, to those of X-aerogels; (b) Desmodur RE for its high-yield conversion to carbon aerogels; and (c) Desmodur N3200 as a typical example for the gelation of diisocyanates.

Desmodur N3300A:

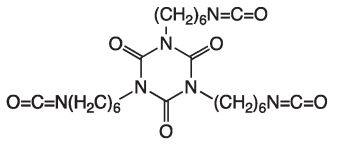

Desmodur RE:

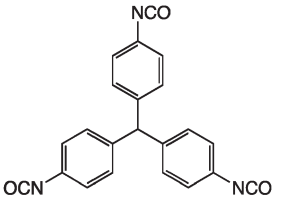

Desmodur N3200:

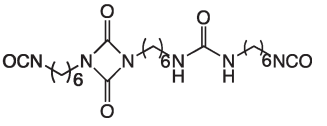

2. Experimental Section

Materials. Monomers Desmodur N3300A triisocyanate, Desmodur RE triisocyanate, Desmodur N3200 diisocyanate, toluene diisocyanate (Mondur TD), and MDI (Mondur CD) were donated generously from Bayer Corporation. Figures S.1−S.3 in Supporting Information provide detailed spectroscopic characterization of all three monomers (mass and infrared spectra, ^{13}C and ^{15}N NMR). All monomers except Desmodur RE are supplied in neat form and were used as received. Desmodur RE is supplied as a solution in ethyl acetate, which was removed with a rotary evaporator before use. Anhydrous acetone was produced from lower grade solvent by distilling over P_2O_5. Triethylamine (99% pure) was purchased from ACROS and was distilled before use.

(16) Fischer, F.; Rigacci, A.; Pirard, R.; Berthon-Fabry, S.; Achard, P. *Polymer* **2006**, *47*, 7636–7645.
(17) Lee, J. K.; Gould, G. L.; Rhine, W. *J. Sol-Gel Sci. Technol.* **2009**, *49*, 209–220.
(18) Wicks, Z. W., Jr.; Jones, F. N.; Pappas, S. P. *Organic Coatings, Science and Technology*, 2nd ed.; Wiley-Interscience: New York, NY, 1999; Chapter 10, p 180.
(19) Odian, G. *Principles of Polymerization*, 4th ed.; Wiley-Interscience: New York, NY, 2004; pp 130−132.

Polyurea aerogels of different densities were prepared by varying the concentration of the monomer by first dissolving 1.375 g, 2.75 g, 5.5 g, 11.0 g, 16.5, or 33 g of Desmodur N3300A in a constant volume (94 mL) of dry acetone. (The seemingly arbitrary choice of monomer and solvent amounts bares no particular significance and stems from the fact that the method described here evolved from previous work with isocyanate cross-linked aerogels;[7−9] what matters is the molar concentrations of the individual components.) Subsequently, for each monomer concentration 1.5, 3.0, or 4.5 mol equiv of water was added, and sols were obtained by adding triethylamine at 0.3%, 0.6%, or 0.9% (w/w) relative to the total weight of the isocyanate monomer plus solvent. The final N3300A monomer concentrations were approximately 0.029 M, 0.056 M, 0.11 M, 0.21 M, 0.30 M, and 0.52 M, respectively. Thus, in a typical procedure, 1.375 g (0.0028 mol) of N3300A was dissolved in 94 mL of dry acetone, 1.5 mol equival of water (0.073 mL, 0.0042 mol) was added, and finally the sol was obtained by adding 0.26 mL of triethylamine (0.3% w/w as defined above). The sol was shaken vigorously, and it was poured into polypropylene syringes used as molds (AirTite Norm-Ject syringes without needles purchased from Fisher, Part No. 14-817-31, 1.40 mm i.d.). The top part of the syringes was cut off with a razor blade, and after the syringes were filled with the sol, it was covered with multiple layers of Parafilm, and the solutions were left to gel. The particular sol of our example gelled in approximately 24 h. The gelation time (defined as the point when a sol does not move by mild shaking) depends on the concentration of the monomer, water, and the catalyst and varies from 24 h to approximately 5 min (at the highest concentrations of all three). For direct comparison, gels with other isocyanates (Desmodur RE, Desmodur N3200, and Mondur TD) were formulated by varying the amount of the monomer in such a way that the final molar concentrations of the monomers in the sols would be about equal to those used for N3300A. With Desmodur RE triisocyanate it was possible to obtain gels over the entire concentration range used with Desmodur N3300A. Gels from Desmodur N3200 and Mondur TD were obtained only for monomer concentrations above ~0.20 M. All formulations and gelation times are summarized in Tables S.1−S.9 of the Supporting Information. All gels were aged for a day. Subsequently, gels were removed from their molds and were placed individually into fresh acetone, approximately 4× the volume of each gel. The solvent was changed two more times every 24 h. Finally, wet-gels were dried into PUA aerogels with liquid CO_2 in an autoclave, taken out at the end as a SCF. Alternatively, xerogels were obtained by ambient drying of acetone-filled wet-gels, while aerogel-like materials were prepared from the two highest density samples (those made with [N3300A] at 0.3 or 0.5 M) by exchanging acetone with pentane (4 washes), followed by drying at 40 °C under ambient pressure. Relevant properties of xerogels and pentane-dried gels are provided in Table S.10 of the Supporting Information.

Methods and Equipment. Drying with SCF CO_2 was conducted in an autoclave (SPI-DRY Jumbo Critical Point Dryer, SPI Supplies, Inc., West Chester, PA). Samples submerged in the last wash bath were loaded in the autoclave and were extracted at 14 °C with liquid CO_2 until no more solvent (acetone) was washed off. Then the temperature of the autoclave was raised above the critical point of CO_2 (32 °C, 73.8 bar), and the pressure was released isothermally at 40 °C. All dry gels were in cylindrical form so that bulk (envelope) densities (ρ_b) were determined from their mass and volume, which in turn was determined from the geometric dimensions of each sample. Skeletal densities (ρ_s) were determined using helium pycnometry with a Micromeritics AccuPyc II 1340 instrument. Porosities, Π, were determined from the ρ_b and ρ_s values according to $\Pi = 100 \times [(1/\rho_b) - (1/\rho_s)]/(1/\rho_b)$. Surface areas ($\sigma$) by the Brunauer−Emmett−Teller (BET) method were determined by nitrogen sorption porosimetry using a Micromeritics ASAP 2020 surface area and pore distribution analyzer. Samples for surface area and skeletal density determinations were outgassed for 24 h at 80 °C under vacuum before analysis. PUA aerogels were characterized chemically by infrared spectroscopy (IR) in KBr compressed pellets using a Nicolet-FTIR model 750 spectrometer and by solids ^{13}C NMR spectroscopy with samples ground into fine powders and packed into 7 mm rotors, using a Bruker Avance 300 spectrometer with 75.475 MHz carbon frequency, magic angle spinning (7 kHz), broad-band proton suppression, and the CPMAS TOSS pulse sequence for spin sideband suppression. ^{13}C NMR spectra were externally referenced to the carbonyl of glycine (176.03 ppm relative to tetramethylsilane). Scanning electron microscopy (SEM) was conducted with samples coated with Au−Pd using a Hitachi S-4700 field emission microscope. X-ray photoelectron spectroscopy (XPS) was conducted with a Kratos Axis 165 photoelectron spectrometer. Samples were presputtered with Ar ions for 1 min prior to analysis. X-ray diffraction (XRD) was conducted using a Scintag 2000 diffractometer with Cu Kα radiation and a proportional counter detector equipped with a flat graphite monochromator. Degrees of crystallinity for the various PUA aerogels were calculated by drawing the baseline (amorphous halo) across the entire diffractogram passing just underneath the diffraction peaks and dividing the area under the peaks left out of the amorphous halo over the total area under the diffractogram. The fundamental building blocks of the aerogel microstructures were probed with ultrasmall- and small-angle neutron scattering (USANS and SANS). USANS measurements were performed at the National Institute of Standards and Technology Center for Neutron Research (NCNR) using the BT-5 Perfect Crystal SANS instrument,[20] while SANS measurements were performed at the NCNR, employing the NG7, 30-m SANS instrument,[21] and at the Manuel Lujan Jr. Scattering Center of the Los Alamos National Laboratory, using the time-of-flight, low-Q diffractometer (LQD).[22] The combination of instruments allowed probing of structural features in the range of 0.001−20 μm. The scattering data are reported in the absolute units of differential cross section per unit volume (cm^{-1}) as a function of Q, the momentum transferred during a scattering event. In all cases, data were reduced by conventional methods and corrected for empty cell and background scattering. In the case of the USANS data, an additional correction was made for slit smearing.[23] Quasistatic mechanical characterization (compression testing) was conducted according to the ASTM D695-02a standard on cylindrical specimens, using a MTS machine (model 810) equipped with a 55 000 lb load cell, as described previously.[24] According to that ASTM standard, the height-to-diameter ratio of the specimen should be 2:1; typical samples were ~1.3 cm in diameter, ~2.6 cm long. Mechanical testing at cryogenic

(20) Barker, J. G.; Glinka, C. J.; Moyer, J. J.; Kim, M. H.; Drews, A. R.; Agamalian, M. *J. Appl. Crystallogr.* **2005**, *38*, 1004–1011.
(21) Glinka, C. J.; Barker, J. G.; Hammouda, B.; Krueger, S.; Moyer, J. J.; Orts, W. J. *J. Appl. Crystallogr.* **1998**, *31*, 430–445.
(22) Seeger, P. A.; Hjelm, R. P., Jr. *J. Appl. Crystallogr.* **1991**, *24*, 467–478.
(23) Kline, S. R. *J. Appl. Crystallogr.* **2006**, *39*, 895–900.
(24) Katti, A.; Shimpi, N.; Roy, S.; Lu, H.; Fabrizio, E. F.; Dass, A.; Capadona, L. A.; Leventis, N. *Chem. Mater.* **2006**, *18*, 285–296.

Scheme 1. Synthesis of Uniform-Density Polyurea (PUA) Aerogels and Photograph of Samples Made of Desmodur N3300A (densities below each sample in mg cm^{-3})

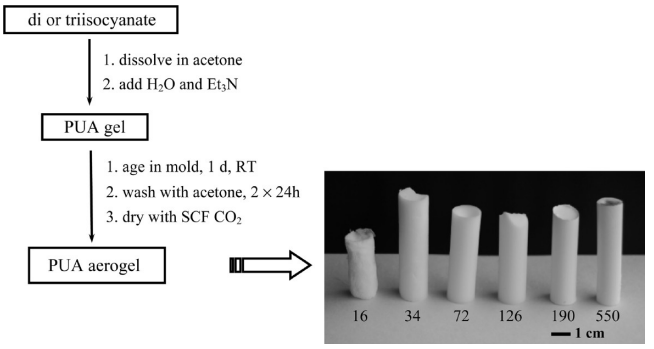

temperatures was conducted by wrapping samples in aluminum foil and dipping in liquid N_2 for 8 h. Samples never came in contact with liquid N_2. Subsequently, samples were unwrapped, quickly placed in the test plate, and tested within 5 s. Thermogravimetric analysis (TGA) was conducted in air or under N_2, with a TA Instruments model 2920 apparatus at a heating rate of 10 °C/min. Carbon aerogels were produced by pyrolysis of PUA samples at 800 °C in a tube furnace under flowing dry Ar (60−65 mL min^{-1}) for 3 h. Elemental analysis for CHN was conducted in house with a Perkin-Elmer CHN analyzer, model 2400, calibrated with acetanilide.

3. Results and Discussion

This section describes the synthesis of PUA aerogels (Section 3.1), their characterization (Section 3.2), and application related properties (Section 3.3).

3.1. Synthesis of PUA aerogels. As summarized in Scheme 1 gelation is induced by adding water and Et_3N in solutions of polyfunctional isocyanates in acetone. Sols become progressively hazy and eventually turn into white gels. Without Et_3N, sols gel in much longer time periods (~3 days), while use of NH_4OH as catalyst accelerates the process causing fast precipitation rather than gelation. Wet-gels were aged to ensure complete reaction of the monomer and solvent-exchanged (washed) with anhydrous acetone. All washes were collected, and no residue was detected, confirming that all isocyanate was incorporated in the gels. All sols able to gel can also be dried into robust aerogel monoliths (see photograph embedded in Scheme 1) by extracting the pore-filling solvent (acetone) with liquid CO_2 taken out at the end as a SCF. Gelation of triisocyanates (aliphatic Desmodur N3300A and aromatic Desmodur RE) takes place with monomer concentrations as low as 0.029 M, while gelation of diisocyanates [aliphatic Desmodur N3200, aromatic Mondur TD (toluene diisocyanate; TDI) and aromatic Mondur CD (4,4′-diphenylmethane diisocyanate; MDI)] takes place only at higher monomer concentrations (> 0.2 M, see Tables S.1−S.9 in Supporting Information). Using Desmodur N3300A triisocyanate as our model system, the gelation time (Figure 1 and Tables S.1−S.6 in Supporting Information) decreases with increasing concentrations of the isocyanate, while the concentration effect of water and the catalyst (Et_3N) is more pronounced at the lower monomer concentrations. Taking

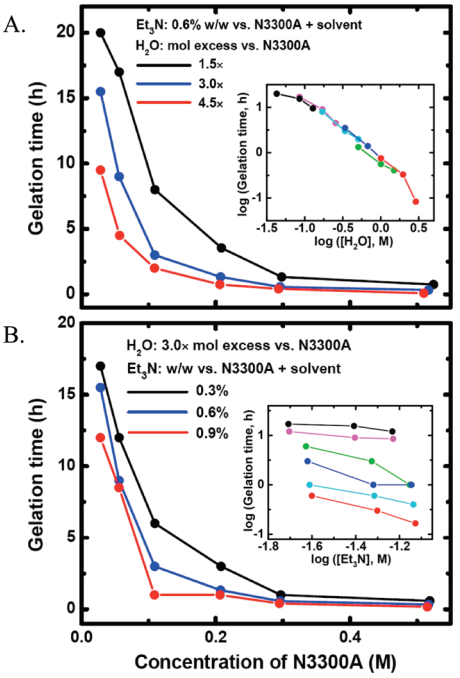

Figure 1. Gelation time as a function of the concentration of Desmodur N3300A triisocyanate. A. For three different water ratios, keeping the catalyst ratio constant. B. For three different catalyst ratios, keeping the water ratio constant. Insets: log−log plots as shown. A. slope = 1.2 ± 0.1. B. slope = 0.9 ± 0.5.

gelation time as a rate indicator, it is found that within the large margin of error associated with the innate system parameters (mainly the concentration of the catalyst),[25] the overall process is first order in both H_2O and Et_3N (see insets in Figure 1), suggesting rate = k[N3300A][H_2O][Et_3N] as the rate law and eq 5 (Scheme 2) as the rate determining step. In that regard, it is noted further that liquids ^{13}C NMR in acetone-d_6 under the gelation conditions for N3300A (Figure S.4 in Supporting Information) shows a gradual decrease of all monomer resonances, with no new peaks assignable to urea. By the gelation point all resonances have been lost. This observation is in accord with the rate-determining step occurring before formation of the carbamic acid. Afterward, reactions should proceed fast to the final product that gets phase-separated (hence the loss of NMR signal), and no accumulation of intermediates is observed.[26] According to that model, PUA elementary (primary) particles should start coming together almost right after the polymer is formed, while further polymerization could still occur at dangling reactive sites (−NH_2 and −NCO) on the surface of newly formed nanoparticles, thus justifying a post-gelation aging step, although the actual need or the effect of the latter was not investigated systematically.

(25) The amine product of the reaction between an isocyanate and water is expected to act as a cocatalyst; therefore, similar log−log plotting for the isocyanate fails to give straight lines, and the rate law is considered first order in [N3300A] based on Scheme 2.

(26) Consideration of Hildebrand solubility parameters for the solvent ($\delta_{acetone}$ = 9.77 cal$^{0.5}$ cm$^{-1.5}$) and polyurea (δ_{PUA} ~ 10 cal$^{0.5}$ cm$^{-1.5}$ (ref 15) taken as approximately equal to that of polyurethanes) would predict high solubility of polyureas; however, the highly cross-linked 3D structure of N3300A-derived polyurea seems to promote early phase separation.

Scheme 2. Gelation Mechanism through Reaction of Isocyanates with Water

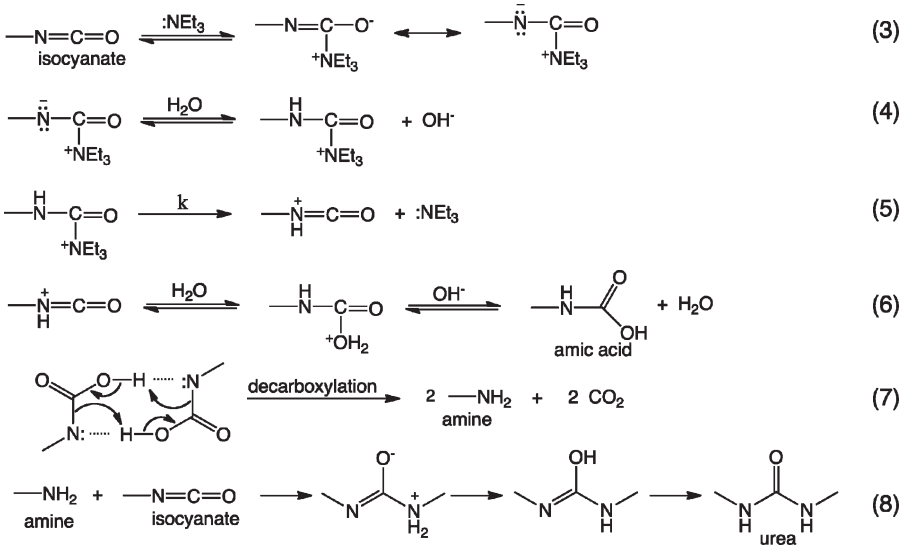

Gelation proceeds qualitatively similarly in acetonitrile, while in DMSO it takes place very fast causing large bubbles of CO_2 to be trapped in translucent gels. Although not pursued further, those DMSO-derived aerogels are interesting materials in their own right as they combine large foam-like macroporosity with nanoporous walls similar to those obtained in acetone or acetonitrile as described in Section 3.2 below. If acetone wet-gels are left to dry under ambient conditions, they undergo extensive shrinkage and yield xerogel-like materials. Alternatively, by applying a method developed previously with polyurea-cross-linked silica aerogels,[27] wet-gels made with the two highest isocyanate concentrations (~0.3 and 0.5 M) and solvent-exchanged with a low vapor pressure/surface-tension solvent like pentane can be dried under ambient pressure at slightly elevated temperature (e.g., 40 °C), yielding materials similar in appearance and properties to those obtained by the SCF CO_2 route. (Selected data for PUA xerogels and pentane-dried samples are listed in Table S.10 of the Supporting Information.) The ambient pressure drying method is currently used for making larger monolithic aerogel pieces for evaluation in certain aeronautical and antiballistic applications. For consistency, however, the presentation below focuses on samples obtained through SCF CO_2 drying.

3.2. Characterization of PUA Aerogels. *3.2a. Chemical Characterization.* The chemical identity of PUA aerogels was probed with IR and solids ^{13}C NMR. The degree of molecular order within the solid framework was investigated with X-ray diffraction (XRD).

Using solids ^{13}C NMR and Desmodur N3300A-derived aerogels as the model system, the NCO carbon resonance at 120.0 ppm has disappeared completely, the resonance of the isocyanurate carbonyl carbon at 149.0 ppm is still present, and the new resonance of the urea C=O carbon has shown up at 159.6 ppm (Figure 2). The relative intensities of the urea, isocyanurate, and aliphatic carbon resonances remain the same irrespective of the relative amounts of water, catalyst, or the concentration of the isocyanate (compare for example Figure 2A,B). Similar data are shown in Figures S.5 and S.6 of the Supporting Information for Desmodur RE triisocyanate- and Desmodur N3200 diisocyanate-derived aerogels.

IR spectroscopic data (Figure 3) agree well with the ^{13}C NMR data. Again, the disappearance of the NCO absorption (2264 cm^{-1}) confirms complete reaction of the NCO groups. The relative intensities of the CH_2 and isocyanurate carbonyl stretches (~2990 cm^{-1} and 1690 cm^{-1}) remain the same between the monomer and the aerogel signifying that trimerization of the NCO groups is not a viable gelation mechanism in our case. Instead, we observe prominent new absorptions at 3373 cm^{-1} and 1563 cm^{-1} assigned to the polyurea NH stretching and bending vibrations, respectively.

XRD of PUA aerogels derived from Desmodur N3300A and Desmodur RE triisocyanates show broad but well-defined diffractions indicating the presence of nanocrystallinity. On the other hand, PUA aerogels derived from N3200 diisocyanate are completely amorphous (Figure 4). The angle of diffraction from N3300A-derived PUA aerogels (21°) is similar to that reported for chemically similar poly(hexamethyleneurea) derived from hexamethylene-1,6-diisocyanate and hexamethylene-1,6-diamine.[28] Neither the degree of crystallinity nor the angle of diffraction (see Table 1) vary with the density of the samples, implying that the average distance between adjacent molecules within the solid PUA framework remains the same or conversely that the polymer chains are packed similarly, irrespective of the gelation time, again consistently with reaction 5 (Scheme 2) being the rate determining step. Overall, the ^{13}C NMR, IR, and XRD data together point to that the concentrations of isocyanate, water, and catalyst have no effect on the

(27) Leventis, N.; Palczer, A.; McCorkle, L.; Zhang, G.; Sotiriou-Leventis, C. *J. Sol-Gel Sci. Technol.* **2005**, *35*, 99–105.

(28) Yadav, S. K.; Khilar, K. C.; Suresh, A. K. *J. Membr. Sci.* **1997**, *125*, 213–218.

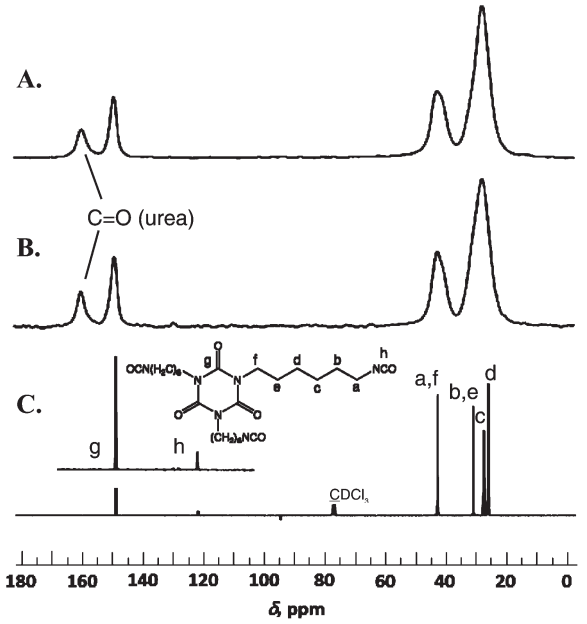

Figure 2. A, B. Solids ^{13}C NMR of two PUA aerogels made with Desmodur N3300A triisocyanate at 0.0285 M (A) and 0.5172 M (B) using in both cases 3.0 mol equival of H_2O and 0.6% (w/w) Et_3N as defined in the Experimental Section. C. Liquids ^{13}C NMR of the monomer in $CDCl_3$.

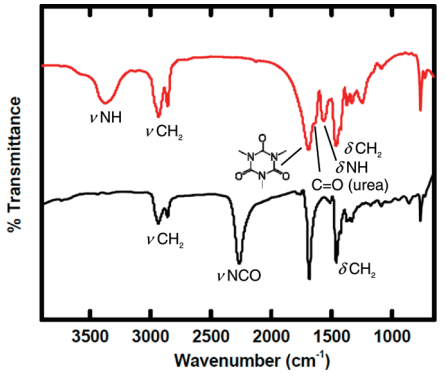

Figure 3. Red (top): Typical infrared (IR) spectrum of a PUA aerogel derived from Desmodur N3300A. Black (bottom): IR of the monomer.

chemical makeup of the PUA aerogels. Therefore, the variation of the nanomorphology as a function of the bulk density that we shall see below cannot be attributed to differences in the chemical composition or the way molecules are packed together. It will have to be attributed to the way elementary particles come together to form the framework.

3.2b. General Material Properties. Those are summarized in Table 1 for samples prepared using the middle formulations of water and triethylamine (i.e., 3.0 molar excess of H_2O and 0.6% (w/w) Et_3N, as detailed in the Experimental Section), for each concentration of the isocyanates (Desmodur N3300A, Desmodur RE, and Desmodur N3200). The complete data for all N3300A samples prepared with all water and catalyst formulations are given in Tables S.11−S.16 of the Supporting Information.

First, all samples shrink relative to their molds. The linear shrinkage of N3300A-derived aerogels is about constant for samples prepared with isocyanate concentrations between

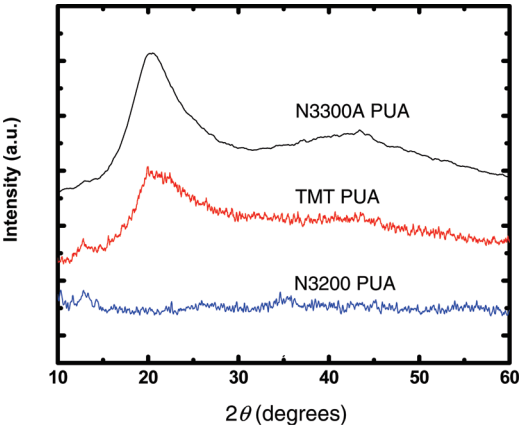

Figure 4. Typical X-ray diffraction patterns of PUA aerogels derived from three different isocyanates as indicated. Data for all formulations are shown in Table 1.

0.029 and 0.30 M and varies between 9 and 15% (Table 1 and Figure 5A). The shrinkage for samples prepared with [N3300A] = 0.52 M is higher, about 25%. By the same token, however, it is noted that the 9−15% shrinkage for the first five samples does not take place during gelation, aging, or washing. Those samples come out of the molds after aging still in tight contact with the mold walls. Shrinkage in the middle- to low-density PUA samples seems to take place exclusively during the SCF CO_2 drying step. Increasing the number of postaging acetone washes from two to four seems to decrease linear shrinkage to between 8 and 10% but does not eliminate it. On the other hand, the larger shrinkage of the samples prepared with [N3300A] = 0.52 M occurs during gelation. Shrinkage is a subject discussed by all previous authors in the area of polyurethane and polyurea aerogels; for isocyanate/amine-derived polyurea aerogels, shrinkage was observed explicitly during aging and drying, it was minimized by increasing the amount of the isocyanate, and therefore it has been attributed to cross-linking of polymeric chains.[17] Clearly, this is not the case in isocyanate/water derived PUAs. On the basis of our observations above, shrinkage for samples prepared with [N3300A] < 0.30 M could be partly attributed to surface tension forces traced to residual gelation water (which is reduced with more post-aging acetone washes), but mostly to the natural tendency of the dry polymer to "settle" in order to maximize van der Waals interactions between noncovalently bonded polymeric segments in close proximity. The disproportionally higher shrinkage (24−27%) of the most concentrated samples ([N3300A] = 0.52 M) is practically invariant of the water and catalyst concentration (see Table S.10, Supporting Information) and, as it was mentioned above, takes place during gelation. The higher shrinkage of those samples has to be attributed to the identity of the elementary building blocks and the way they assemble to form the nanostructure—see Section 3.2c below.

The discontinuity in the shrinkage when [N3300A] > 0.30 M is reflected upon the bulk densities, ρ_b, as expected (Table 1): while up to that point ρ_b varies linearly with the concentration of the isocyanate in the sol (Figure 5A), it appears disproportionally higher beyond that point.

Table 1. Selected Materials Properties of PUA Aerogels Prepared with the Isocyanates Indicated Using the Middle H_2O and Et_3N Formulations, that is, 3.0 mol equiv of Water and 0.6% (w/w) Et_3N (refer to Tables S.1−S.8, Supporting Information)

[isocyanate] in sol (M)	diameter (cm)[a]	linear shrinkage (%)[a,b]	bulk density, ρ_b (g cm^{-3})[a]	skeletal density, ρ_s (g cm^{-3})[c]	crystallinity (%) [2θ]	porosity, Π (% void space)	BET surface area, σ (m^2 g^{-1})	average pore diameter (nm)[d]
				Desmodur N3300A				
0.0285	1.28 ± 0.01	13.3 ± 0.56	0.016 ± 0.000$_4$	1.24 ± 0.23	28 [21.1]	98.6	222.4	53.7 [50.0]
0.0561	1.35 ± 0.01	9.12 ± 0.85	0.034 ± 0.000$_4$	1.31 ± 0.06	34 [20.5]	97.5	243.5	38.9 [39.0]
0.1092	1.27 ± 0.01	14.8 ± 0.18	0.072 ± 0.005	1.21 ± 0.03	33 [20.3]	93.9	234.7	32.3 [32.0]
0.2073	1.32 ± 0.01	10.6 ± 0.18	0.126 ± 0.001	1.30 ± 0.07	35 [20.3, 44]	90.3	169.4	41.6 [41.0]
0.2960	1.27 ± 0.03	14.1 ± 1.78	0.19 ± 0.01	1.21 ± 0.02	35 [20.5, 45]	84.2	67.5	40.7 [41.0]
0.5171	1.11 ± 0.02	25 ± 1.35	0.55 ± 0.03	1.20 ± 0.00$_1$	35 [20.5, 45]	54.1	53.8	38.7 [39.0]
				Desmodur RE				
0.0284	1.29 ± 0.01	13 ± 0.64	0.023 ± 0.002	1.24 ± 0.14	8.2 [23.4, 43.5]	98.1	222.4	12 [11.8]
0.0563	1.21 ± 0.04	18.5 ± 2.7	0.037 ± 0.003	1.30 ± 0.01	9.1 [25.3, 43.5]	97.1	320.7	7.6 [8.4]
0.1099	1.29 ± 0.01	12.8 ± 0.7	0.062 ± 0.005	1.23 ± 0.03	9.0 [24.7, 43.7]	95	6.55	7.5 [8.7]
0.2101	1.28 ± 0.03	13.3 ± 2.1	0.15 ± 0.02	1.24 ± 0.23	12.0 [24.3, 43.9]	87.8	6.49	7.75 [7.6]
0.3019	1.3 ± 0.6	12.4 ± 0.4	0.18 ± 0.01	1.24 ± 0.25	14.9 [20.8, 43.2]	85.7	19.9	10.6 [11.2]
0.5360	1.31 ± 0.01	12.1 ± 0.2	0.25 ± 0.02	1.24 ± 0.28	10.8 [21.2, 43.8]	79.8	3.24	6.6 [7.8]
				Desmodur N3200				
0.2066	1.26 ± 0.01	14.6 ± 1.0	0.175 ± 0.007	1.15 ± 0.01	0.0	84.6	4.3	7.4 [8.2]
0.2955	1.13 ± 0.01	24.7 ± 0.8	0.37 ± 0.01	1.15 ± 0.01	0.0	68.5	12.8	8.5 [9.1]
0.5166	1.05 ± 0.05	14.3 ± 0.9	0.54 ± 0.07	1.15 ± 0.03	0.0	52.7	23.6	12.05 [12.3]

[a] Average of five samples. (Mold diameter: 1.40 cm.) [b] Shrinkage = 100 × (sample diameter − mold diameter)/(mold diameter). [c] Single sample, average of 50 measurements. [d] By the BJH desorption method; in brackets: width at half-maximum.

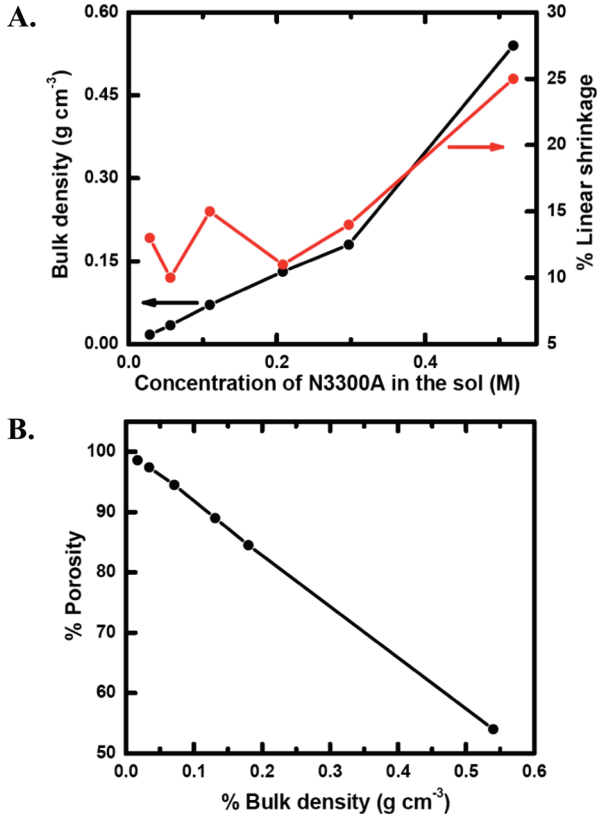

Figure 5. A. Bulk density of PUA aerogels as a function of the monomer concentration in the sol using 3.0 mol equiv of H_2O and 0.6% (w/w) Et_3N as defined in the Experimental Section. B. Correlation of porosity (% v/v of void space) and bulk density.

On the other hand, in agreement with the same chemical composition and packing of the polymer chains within the elementary building blocks, skeletal densities, ρ_s, are all within the range of 1.20−1.30 g cm^{-3}, indicating absence of closed porosity. Consequently, porosities, Π, as % v/v of empty space, formally calculated from the ρ_b and ρ_s values, show the same discontinuity as ρ_b at [N3300A] > 0.30 M (Table 1), so that at the end Π and ρ_b correlate linearly over all formulations (Figure 5B). Finally, BET surface areas (Table 1) are also relatively high (220−250 m^2 g^{-1}) for samples prepared with [N3300A] < 0.11 M, dropping suddenly to 169 m^2 g^{-1} for [N3300A] = 0.21 M and below 70 m^2 g^{-1} for [N3300A] > 0.3 M, suggesting drastic changes in the microstructure.

Table 1 also includes similar data for aerogels derived from aromatic Desmodur RE triisocyanate and aliphatic Desmodur N3200 diisocyanate. Those samples show no identifiable trends in shrinkage, and consequently we observe no sudden jumps in their bulk density or their porosity. Nevertheless, the BET surface areas of the Desmodur RE-derived PUA samples show a sudden drop from ~320 m^2 g^{-1} to the 70−20 m^2 g^{-1} range when [Desmodur RE] > 0.056 M, which is much earlier (density-wise) than what is observed in the N3300A-derived samples. (As we saw above, a similar drop in surface area was observed at [N3300A] > 0.3 M.) Further, it is noteworthy that despite high porosities (e.g., 85% v/v), the BET surface area of the Desmodur N3200-derived samples is uniformly very low, < 20 m^2 g^{-1}, over all possible densities. Considered together, shrinkage, porosity, and surface area data for all three kinds of isocyanates suggest changes in the microstructure as a function of the density and the chemical identity of the monomer (rigid vs flexible, di- vs triisocyanate). That necessitates a detailed view of the micromorphology/pore structure of the three different kinds of PUA aerogels.

3.2c. Microscopic Characterization. The structure of PUA aerogels as a function of their preparation conditions was probed semiquantitatively with N_2 sorption porosimetry and SEM and quantitatively with SANS/USANS.

By SEM (Figure 6) all N3300A derived samples appear macroporous, with voids larger than 50 nm. This macroporosity is clearly evident in the N_2 sorption data

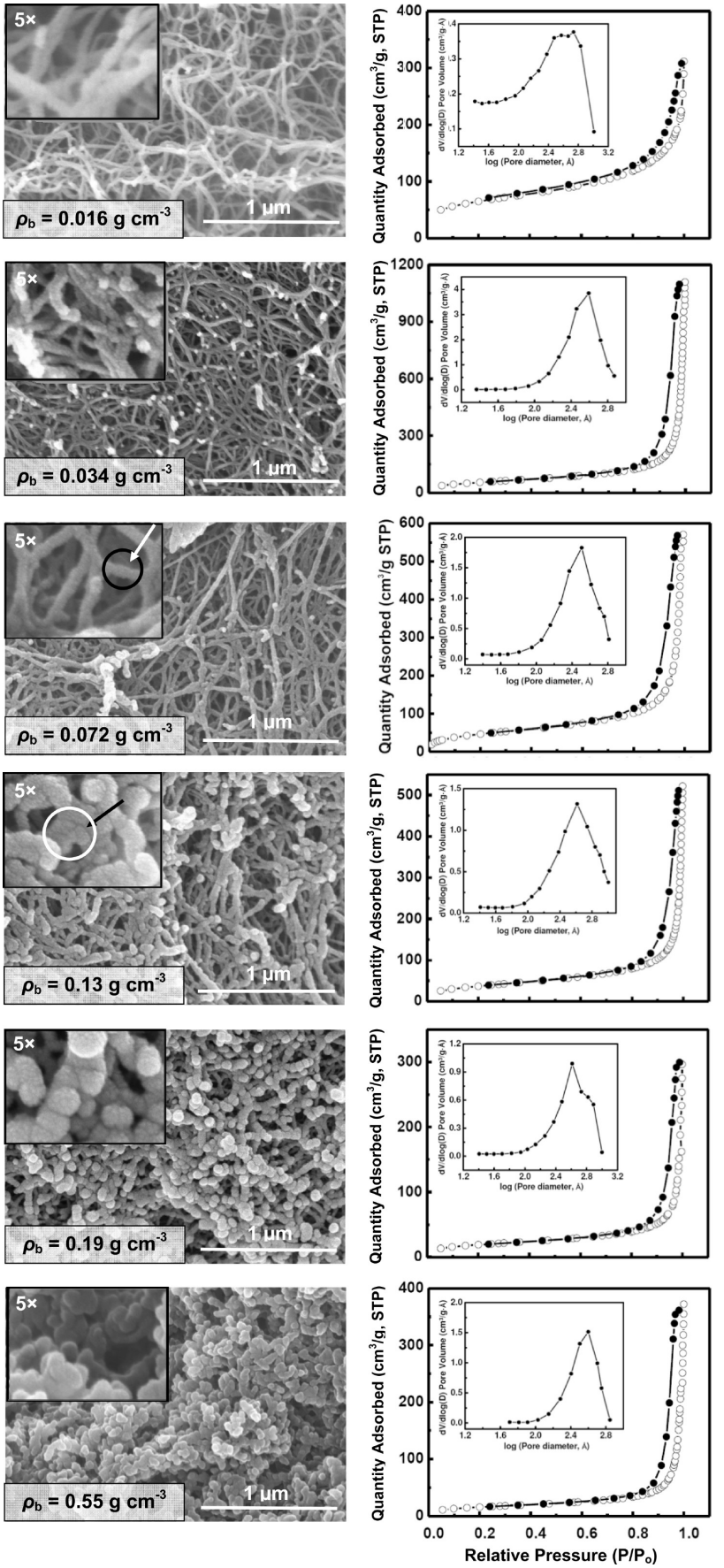

Figure 6. Scanning electron microscopy (SEM) and N_2 sorption porosimetry as a function of density of PUA aerogels derived from Desmodur N3300A triisocyanate using 3.0 mol equiv of H_2O and 0.6% (w/w) Et_3N as defined in the Experimental Section. (For the effect of water and catalyst concentration on the microstructure at constant isocyanate concentration refer to Figure S.7 in Supporting Information).

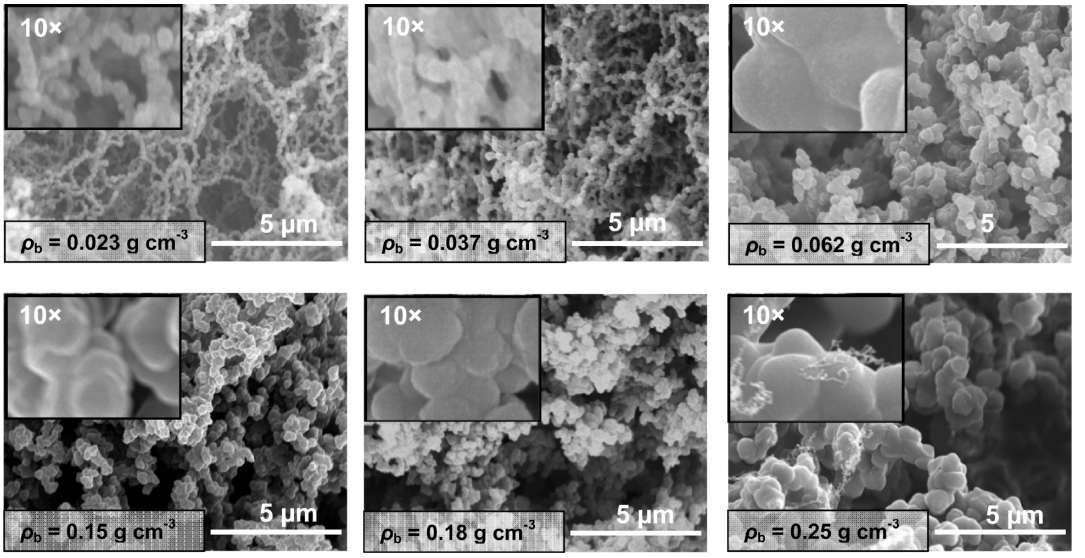

Figure 7. SEM as a function of density of PUA aerogels derived from Desmodur RE triisocyanate using 3.0 mol equiv of H_2O and 0.6% (w/w) Et_3N as defined in the Experimental Section.

included in Figure 6: the adsorption branch rises sharply above relative pressure (P/P_0) of 0.9, and it does not reach saturation at the condensation point of N_2 at (P/P_0) $\sim$ 1. The presence of hysteresis loops, however, implies the presence of some mesoporosity as well. BJH-desorption plots (insets in Figure 6) are quite broad, and they look like overlapping pore-size distributions (only the absolute maximum is reported in Table 1).

As far as the skeletal framework is concerned, according to Figure 6, at low densities (e.g., <0.072 g cm^{-3}) N3300A-derived PUA aerogels are fibrous, but they clearly turn particulate at higher densities (e.g., at 0.55 g cm^{-3}). The nanomorphology at each density depends only on the concentration of the isocyanate in the sol, and it is independent of the concentration of water or the catalyst (see Figure S.7, Supporting Information). The morphology switch seems to take place in the 0.13−0.19 g cm^{-3} range. At higher magnification (Figure 6, insets) fibers at first (0.016 g cm^{-3}) appear relatively smooth but "knotty", and later (e.g., at 0.034 g cm^{-3}, or at 0.072 g cm^{-3}) they are clearly rough, as if they consist of agglomerations of particles. This situation becomes very pronounced at 0.13 g cm^{-3}; particulated strings seem to dominate at 0.19 g cm^{-3}, and by 0.55 g cm^{-3} there is practically no remnance of any fibrous structure. Upon a more careful look at the 0.072−0.19 g cm^{-3} samples, strings appear consisting of disk-like structures (indicated by circles and arrows) stuck together as in a spine. The idenity of those disk-like structures as independent building blocks is confirmed by SANS/USANS below.

By changing the triisocyanate from flexible aliphatic N3300A to rigid aromatic Desmodur RE, Figure 7 shows an analogous behavior: at low densities the structure starts fibrous, progressively turning particulate. That change takes place at much lower densities than in N3300A-derived aerogels; by 0.062 g cm^{-3} the RE-derived structure is particulate. The morphology of the Desmodur RE-derived fibers is different from those observed with N3300A aerogels; they consist of well-defined beads connected with narrow necks (see the 0.023 g cm^{-3} sample in Figure 7). As the density increases to 0.037 g cm^{-3}, the particle size remains about the same, but the interparticle necks have become wider; upon further increase in density the material appears nanoparticulate with a very faint remnance of strings, if any.

With N3200-aerogels (Figure 8) the situation resembles the higher density Desmodur RE samples (refer to Figure 7); namely, the structure is particulate, but overall particles now are larger than those of the RE aerogels by a factor of 2×.

The makeup of the features observed by SEM would give information about the gelation process postphase separation. Since Desmodur N3300A-derived PUA aerogels show a broader range of nanomorphologies than those from Desmodur N3200 and Desmodur RE, they were chosen for further quantitative investigation with SANS/USANS at length scales extending from 1 nm to 20 μm (Figure 9).

By SANS/USANS, N3300A-derived PUA aerogels display density-dependent multilength scales with at least two power-law regions (linear sections in the log−log plots of Figure 9). The solid lines in Figure 9 are fits to the Unified Model of G. Beaucage (eq 9),[29] which distinguishes Guinier regimes overlapping significantly with Porod (power law) regimes and is used for analyzing data from multiscale structures such as foams.

$$I(Q) = \sum_i G_i \exp\left(\frac{-Q^2(R_g)_i^2}{3}\right) + B_i \exp\left(\frac{-Q^2(R_g)_{i+1}^2}{3}\right) \times \left\{\left[\frac{\mathrm{erf}(Qk(R_g)_i}{\sqrt{6}}\right]^3/Q\right\}^{\beta_i} \quad (9)$$

$I(Q)$ is the scattering intensity, "i" refers to the structural level, $G_i = N_i(\Delta\rho)_i^2V_i^2$, $B_i = 2\pi(\Delta\rho)_i^2N_iS_i$, N_i is the

(29) (a) Beaucage, G. *J. Appl. Crystallogr.* **1995**, *28*, 717–728. (b) Beaucage, G. *J. Appl. Crystallogr.* **1996**, *29*, 134–146.
(30) Koberstein, J. T.; Morra, B.; Stein, R. S. *J. Appl. Crystallogr.* **1980**, *13*, 34–45.

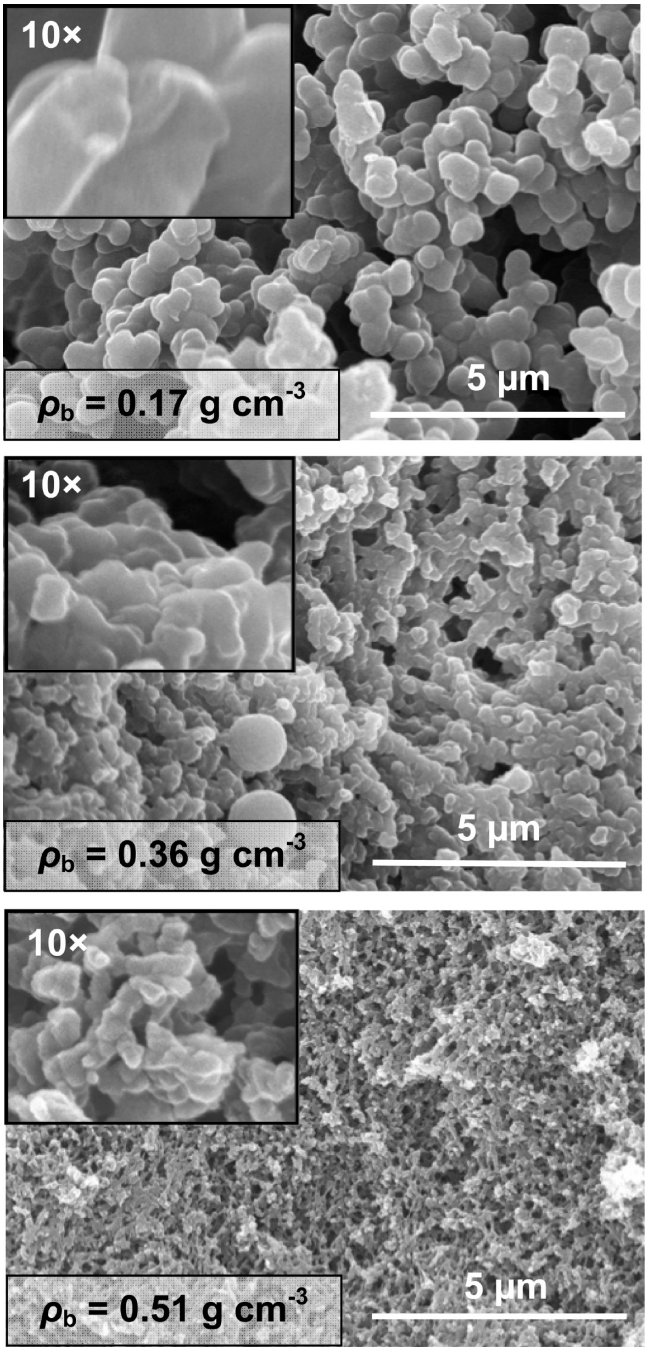

Figure 8. SEM as a function of density of PUA aerogels derived from Desmodur N3200 diisocyanate using 3.0 mol equiv of H_2O and 0.6% (w/w) Et_3N as defined in the Experimental Section.

number density of primary particles (i.e., the number of scatterers per unit volume), $(\Delta\rho)_i$ is the difference in scattering-length density between scatterers and the me dium, S_i is the surface area of a scatterer, V_i is an average particle volume, k is an empirical constant (for polymeric mass fractals $k = 1.06$), and β_i is the scattering exponent related to the fractal dimensions.[29] Data derived from Figure 9 are summarized in Table 2.

To facilitate matching of data with scattering features (see footnotes in Table 2), scattering profiles in Figure 9 have been divided in several regions, starting with Porod scattering as Region I at high Q values. In that power-law region, lower density aerogels ($\leq$0.072 g cm^{-3}) display exponents slightly more negative than −4.0, indicating that the smallest elementary building blocks of the aerogels (primary particles) have fuzzy interfaces; namely, they display variations in density across their interfaces. Presently, the origin of that fuzziness is unclear; frequently it comes from core−shell structures, but in this case that is improbable. The interfacial thicknesses, t, are calculated via eq 10,

$$t = (2\pi)^{0.5}\sigma \tag{10}$$

by assuming Gaussian distribution of matter at the nanoparticle interface with standard deviation σ, and fitting the scattering intensity to the modified Porod's law (eq 11).[30]

$$I(Q) = 2\pi N(\Delta\rho)^2 SQ^{-4}\exp[-\sigma^2Q^2] \tag{11}$$

All t fall at around 1 nm (Table 2), setting that as the lowest limit for the size of the smallest elementary building blocks. Higher density samples (> 0.13 g cm^{-3}) give Region I exponents equal to −4.0 indicating sharp (abrupt) interfaces. In Region II, all samples display a Guinier "knee", which is indicative of a fundamental length-scale and is attributed to the primary particles forming the materials. Analysis according to the Unified Model provides the radius of gyration (R_g), where for monodispersed spherical particles $R_g \approx 0.77R$ (R is the radius of the particles).[31] However, the monotonic falloff in Region I implies polydispersity (monodisperse particles give rise to "ripples" in that region). Therefore, R_g values were analyzed further assuming particle polydispersity and log-normal distributions for the particle size. According to that analysis the radius of gyration is related to the mean radius of the scatterers by eq 12,[32]

$$(R_g)^2 = (3/5)(\langle R^8\rangle/\langle R^6\rangle) \tag{12}$$

where $\langle R^n\rangle = m^n\exp(n^2\sigma^2/2)$, m is related to the mean, by $\langle R\rangle = m\exp(\sigma^2/2)$, and σ is the standard deviation of the log-normal distribution. Table 2 provides both the R_g values and the mean primary particle radii, $\langle R\rangle$, as well as the particle size distribution (PSD) in terms of m and σ. Overall, the elementary building blocks of all samples, fibrous or particulate, are primary particles with radii increasing with ρ_b from ~3 to 12.5 nm. That increase in size may be attributed either to the length of the polymer (degree of polymerization) before phase separation or to monomer reacting and accumulating on the surface of newly formed primary particles before they assemble to higher structures. Both explanations are quite probable; the first one is straightforward, while the second one finds support from the smoothing of the surface fuzziness of the primary particles with increasing isocyanate concentration in the sol, and from the neck broadening in the case of the Desmodur RE-derived samples (Figure 7: refer to the wider necks in the 0.037 g cm^{-3} samples relative to the 0.023 g cm^{-3} ones).

(31) Guinier, A; Fournet, G. *Small-Angle Scattering of X-rays*; John Wiley and Sons: New York, NY, 1955.
(32) Beaucage, G.; Kammler, H. K.; Pratsinis, S. E. *J. Appl. Crystallogr.* **2004**, *37*, 523–535.

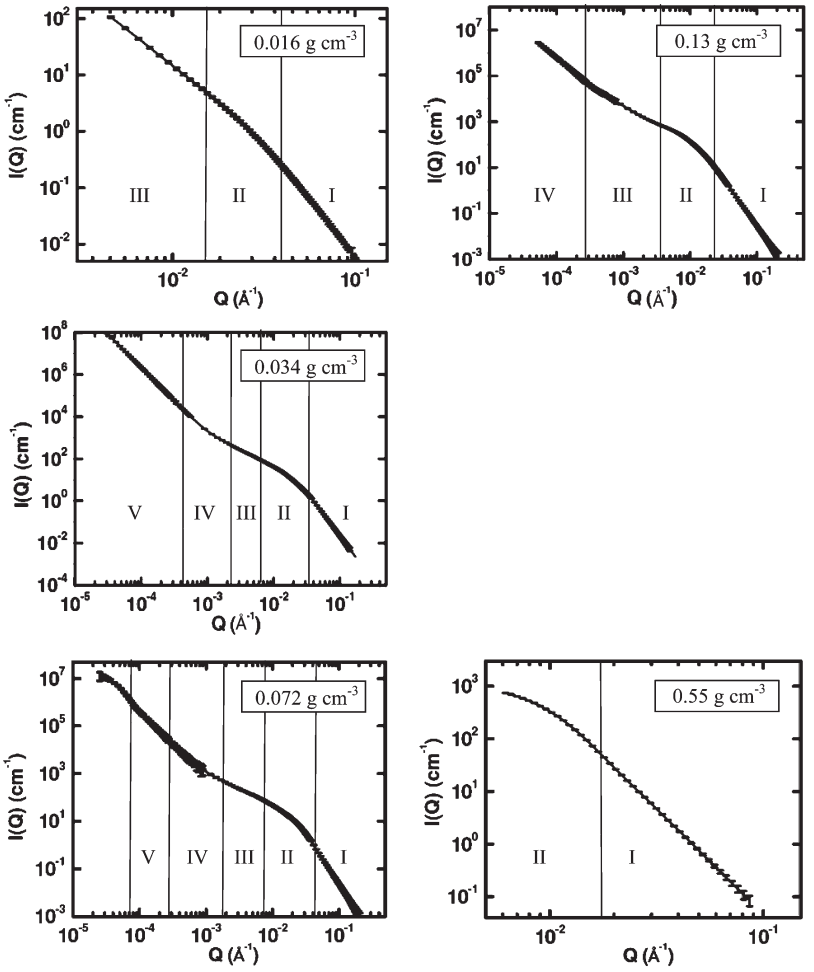

Figure 9. SANS/USANS data as a function of PUA aerogels derived from Desmodur N3300A triisocyanate using 3.0 mol equiv of H_2O and 0.6% (w/w) Et_3N as defined in the Experimental Section. Vertical lines separate scattering profiles in regions that provide the data presented in Table 2.

Table 2. Results from Small Angle Neutron Scattering (SANS/USANS) of Polyurea Aerogels Derived from Desmodur N3300A

	primary particles				secondary structures		
bulk density (ρ_b, g cm^{-3})	t (nm)	R_g (nm)	$\langle R \rangle$ (nm)	PSD (m; σ)	R_g (nm)	D_m	D_s
0.016[a]	0.8 ± 0.1	7.4 ± 0.9[d]	3.5[d]	3.2; 0.39	[n]	2.51 ± 0.06[e]	[n]
0.034[b]	1.1 ± 0.1	12.5 ± 0.2[d]	5.1[d]	4.7; 0.42	91 ± 3[f]	2.2 ± 0.1[g]	2.85 ± 0.02[h]
0.072[b]	0.9 ± 0.02	7.0 ± 0.5[d]	3.0[d]	2.7; 0.41	166 ± 20[j]	2.0 ± 0.3,[i] 2.74 ± 0.02[k]	
0.13[b]	[c]	21.7 ± 0.1[d]	10.4[d]	9.7; 0.39	805 ± 145[l]	1.98 ± 0.02,[l] 2.35 ± 0.07[m]	
0.55[a]	[c]	20.9 ± 0.5[d]	12.5[d]	12; 0.34	[n]	[n]	[n]

[a] By SANS. [b] By SANS/USANS. [c] Abrupt interface. Refer to Figure 9. [d] Refer to Figure 9. From the Guinier Region II in all samples. [e] Refer to Figure 9. Sample 0.016, Region III. [f] Refer to Figure 9. Sample 0.034, Region IV. [g] Refer to Figure 9. Sample 0.034, Region III. [h] Refer to Figure 9. Sample 0.034, Region V. [i] Refer to Figure 9. Sample 0.072, Region III. [j] Refer to Figure 9. Sample 0.072, Region IV. [k] Refer to Figure 9. Sample 0.072, Region V. [l] Refer to Figure 9. Sample 0.13, by deconvolution of Region III. [m] Refer to Figure 9. Sample 0.13, Region IV. [n] Q was not extended to low enough values to obtain data for these quantities.

In Region III, samples exhibit power law scattering again, with exponents between −2 and −3, indicating that primary particles form mass fractal secondary aggregates. The mass-fractal dimensions, D_m, are given by the slopes. The Guinier Region IV provides a second radius of gyration that is related (via $R_g \approx 0.77R$) to the radii of the secondary aggregates formed by the primary particles. Overall, with increasing ρ_b (and therefore primary particle size), the R_g values of the secondary aggregates increase (from 91 to 805 nm) while their fractal dimensions decrease (from 2.51 to 1.98) indicating that larger primary particles form larger but less dense secondary aggregates. In that regard, the 0.072 g cm^{-3} and the 0.13 g cm^{-3} samples are particularly interesting. Here specifically, since both $D_m \approx 2.0$, it is concluded that primary particles are aggregating to form disk-like secondary structures (with R_g equal to 166 and 805 nm, respectively). Disk-like structures are in fact visible in SEM (Figure 9, insets, disks are pointed at by arrows and circles), and they are stuck to form strings.

Indeed, similar analysis in the remaining regions of Figure 9 shows that secondary aggregates do assemble to form higher fractal agglomerates (fibers, Figure 6). Thus, in the sample with $\rho_b = 0.034$ g cm^{-3}, the exponent in

power-law Region V is >3, indicating surface fractals with fractal dimension $D_s = 2.85 \pm 0.02$. On the basis of the range of Q where that fractality appears and by considering the SEM of that sample (Figure 6), surface fractality should be created by the fiber entanglement, whereas, apparently, an attempt to measure the surface area would depend on the surface area of the probe. In the case of the 0.072 g cm^{-3} sample, strings consisting of disk-like structures form mass fractals ($D_m = 2.74$), which are more dense than those formed by the 0.13 g cm^{-3} samples ($D_m = 2.35$).

The most dense samples ($\rho_b = 0.55$ g cm^{-3}) appear as a classic aerogel: by SEM they appear as a collection of nanoparticles, while SANS indicates that they consist of smooth primary particles ($\langle R \rangle = 12.5$ nm) that assemble into larger secondary clusters (by SEM).

Putting all the chemical and microscopic evidence together, the structure of the PUA aerogels seems to be controlled by phase separation. Since Desmodur N3200 diisocyanate yields a flexible, more soluble linear polymer, phase separation takes place later leading to larger particles that tend to "collapse" to maximize van der Waals interactions, hence, the overall smoother microstructure observed in SEM (Figure 8) and the very small BET surface areas (Table 1). Triisocyanates develop a 3D molecular structure leading to earlier phase separation and smaller particles. The evolution of the microstructure with increasing density (SEM, Figures 6 and 7) could have been explained by particles accumulating on newly formed strings. However, SANS/USANS data clearly show that this is not the case: primary particles assemble into secondary aggregates, which in turn are shown quantitatively (whenever USANS data are available) to form higher fractal agglomerates (surface or mass). This hierarchical structure from primary particles to secondary globules or disks to larger string-like aggregates precludes a particle-on-fiber growth model. Assembly of secondary particles into organized structures like fibers or strings should proceed via a reaction-limited cluster aggregation mechanism;[33] it is speculated that since particles are expected to be chemically connected through reaction of surface −NCO on one particle with $-NH_2$ or −NHCONH− groups on another, at low isocyanate concentrations formation of strings versus globules may be favored for steric reasons: in globules, the chemical energy stabilization by formation of interparticle urea bridges would be compromised by the energy to overcome crowding. At intermediate isocyanate concentrations, disk-like objects maximize chemical bond formation by sticking on top of one another in a spine-like fashion. At higher isocyanate concentrations, or when the polymer solubility is low, the fast rise in the concentration of nanoparticles may lead to a diffusion-limited cluster−cluster aggregation mechanism and the structure turns into nanoparticulate/globular (as in the 0.55 g cm^{-3} sample).[34] Both the smoothing of the primary particles and their size increase at higher N3300A concentrations (Table 2), as well as the SEM data for the Desmodur RE-derived PUAs, indicate that all mechanisms may be convoluted with monomer-cluster growth processes.[35] Nanoparticulate structures are more prone to shrink to maximize noncovalent interactions between polymer chains.

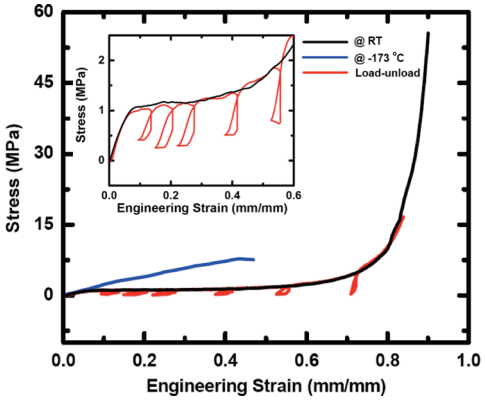

Figure 10. Quasi-static (strain rate = 0.05 s^{-1}) compression testing of PUA aerogel monoliths ($\rho_b = 0.13$ g cm^{-3}) derived from Desmodur N3300A triisocyanate, under the conditions shown within the frame.

3.3. Macroscopic Properties Related to the Nanostructure. As evident from the Introduction, organic aerogels are mainly pursued for thermal insulation and for their conversion to carbon aerogels as electrodes for fuel cells and supercapacitors and as catalyst supports.[36] As it will be discussed below, conversion of PUA aerogels to carbons is particularly important because of its relevance to the synthesis of nanoporous metals and ceramics, while, from a fundamental perspective, one line of reasoning suggests that since the exceptional mechanical properties of polymer-cross-linked aerogels are traced to their conformal polymer coating, if aerogels consist only of polymer with similar nanostructure and interparticle connectivity as in polymer cross-linked aerogels, they should possess similar mechanical properties. According to Section 3.2c above, PUA aerogels appear to satisfy this condition, setting the stage for a detailed study of their mechanical behavior.

3.3a. Mechanical characterization. For direct comparison with polyurea-cross-linked inorganic aerogels (silica and vanadia, abbreviated as X-silica and X-vanadia), this study focuses on compression testing. Desmodur N3300A-derived aerogels were used again as the model system, and properties such as stiffness (quantified by Young's modulus, E), yield strength at 0.2% offset strain, ultimate compressive strength at maximum strain (UCS) and toughness (T, quantified by the specific energy absorption) were evaluated as a function of the density at both room and cryogenic temperatures under quasi-static conditions (i.e., low strain rates).

Figure 10 shows typical stress−strain curves of cylindrical specimens under compression at both room and

(33) Keefer, K. D.; Schaefer, D. W. *Phys. Rev. Lett.* **1984**, *53*, 1383–1386.
(34) Witten, T. A., Jr.; Sander, L. M. *Phys. Rev. Lett.* **1981**, *47*, 1400–1403.
(35) (a) Keefer, K. D.; Schaefer, D. W. *Phys. Rev. Lett.* **1986**, *56*, 2376–2379. (b) Keefer, K. D.; Schaefer, D. W. *Phys. Rev. Lett.* **1986**, *56*, 2199–2202.
(36) (a) Smirnova, A.; Ding, X.; Hara, H.; Vasiliev, A.; Sammes, N. *Int. J. Hydrogen Energy* **2005**, *30*, 149–158. (b) Kwon, O. J.; Jung, Y. S.; Kim, J. H.; Oh, S. M. *J. Power Sources* **2004**, *125*, 221–227. (c) Fialkov, A. S. *Russ. J. Electrochem.* **2000**, *36*, 345–366.

Table 3. Mechanical Characterization Data under Quasi-Static Compression at Room (23 °C) and Cryogenic (−173 °C) Temperatures of Desmodur N3300A-Derived PUA Aerogels[a]

bulk density (ρ_b, g cm^{-3})	strain rate (s^{-1})	Young's Modulus (E, MPa)	speed of sound (m s^{-1})	yield stress at 0.2% offset strain (MPa)	ultimate strength (UCS, MPa)	ultimate strain (%)	Poisson ratio at strain: 5% [70% or 40%][b]	specific energy abs. (T, J g^{-1})[c]
				23 °C				
				polyurea aerogels				
$0.016 \pm 0.000_4$		[d]	[d]	[d]	[d]	[d]	[d]	[d]
$0.034 \pm 0.000_4$	0.05	3.868	337	0.12	3.9 ± 0.5	90 ± 1	0.20 ± 0.03 [0.16 ± 0.01]	9.7
0.072 ± 0.005	0.05	7.027	312	0.20	45	92	0.21 ± 0.02 [0.16 ± 0.02]	22.75
0.126 ± 0.001	0.05	20 ± 3	398	$1.1 \pm 0.1_4$	54 ± 3	$91 \pm 0._0$	0.23 ± 0.03 [0.17 ± 0.04]	21 ± 9
0.19 ± 0.01	0.05	33 ± 2	416	1.6 ± 1.1	106 ± 7	88 ± 2	0.21 ± 0.02 [0.18 ± 0.03]	26.0
0.55 ± 0.03	0.05	300 ± 47	738	13 ± 2	631 ± 39	88 ± 3	0.23 ± 0.18 [0.22 ± 0.04]	91 ± 5
				X-silica aerogels				
0.548 ± 0.005	0.005	233 ± 8	652	6.0 ± 0.6	186 ± 22	68 ± 1	0.18	47.0 ± 0.7
				X-vanadia aerogels				
0.436 ± 0.004	0.005	206 ± 14	687	5.6 ± 0.4	371 ± 32	91 ± 2	0.21 ± 0.02 [0.23 ± 0.03]	192 ± 12
				Cryogenic Temperature				
				polyurea aerogels (−173 °C)				
$0.016 \pm 0.000_4$		[e]	[e]	[e]	[e]	[e]	[e]	[e]
$0.034 \pm 0.000_4$		[e]	[e]	[e]	[e]	[e]	[e]	[e]
0.072 ± 0.005	0.05	2.77 ± 0.04	196	0.10 ± 0.03	10 ± 1	72.0 ± 0.2	0.30 ± 0.03 [0.28 ± 0.04]	33.25
0.126 ± 0.001	0.05	25 ± 7	445	3.0 ± 0.2	8.0 ± 0.1	45.0 ± 0.1	0.31 ± 0.04 [0.28 ± 0.04]	28 ± 2
0.19 ± 0.01	0.05	75.5 ± 0.5	632	9 ± 1	19 ± 4	$50.0 \pm 0.0_3$	0.32 ± 0.04 [0.29 ± 0.06]	26 ± 2
0.55 ± 0.03	0.05	490 ± 8	943	50 ± 3	100 ± 6	42.0 ± 0.2	0.33 ± 0.05 [0.31 ± 0.05]	$54.6 \pm 0.0_1$
				X-silica aerogels (−196 °C)				
0.548 ± 0.005	0.05	635 ± 8	1076	19.9 ± 1.8	107 ± 12	16 ± 1	0.20 ± 0.03[f]	9.9 ± 0.6
				X-vanadia aerogels (−196 °C)				
0.444 ± 0.004	0.05	438 ± 11	993	13.6 ± 1.5	183 ± 17	72 ± 3	0.27 ± 0.06[f]	163 ± 2

[a] Average of three samples unless no range given, in which case only a single sample was tested. [b] For samples tested at room temperature, Poisson ratios in brackets were calculated at the beginning of the densification range (at 70% strain); for samples tested at −173 °C those numbers are at 40% strain, because that is the minimum strain that could be tolerated by all samples (see adjacent "ultimate strain" column). [c] Calculated at ultimate strain. [d] Too weak to accept load. [e] Too fragile to handle at cryogenic temperature: samples crumbled under minimum stress. [f] Not measured.

Table 4. Selected Materials Properties of Desmodur N3300A-Derived Aerogels after Full Compression

bulk denisty before compression, ρ_b (g cm^{-3})[a]	diameter after full compression (cm)[b]	bulk density after compression ρ_b (g cm^{-3})[c]	skeletal density ρ_s (g cm^{-3})[d]	porosity, Π (% v/v void space)	BET surface area, σ (m^2 g^{-1})[e]	average pore diameter
0.072 ± 0.005	1.4 ± 0.25	0.35 ± 0.32	1.22 ± 0.12	71.6	67.8	8.5 [122]
0.126 ± 0.001	1.42 ± 0.18	0.55 ± 0.14	1.22 ± 0.01	54.8	8.22	31.3 [491]
0.19 ± 0.01	1.42 ± 0.13	0.66 ± 0.51	1.24 ± 0.05	46.7	0.9	25.3 [3171]
0.55 ± 0.03	2.31 ± 0.07	0.76 ± 0.38	1.25 ± 0.08	39.5	5.3	29.7 [393]

[a] Samples prepared using middle H_2O/Et_3N formulation: 3.0 mol excess of H_2O, 0.6% (w/w) Et_3N. (See Tables 3 and S.11-S.16 in Supporting Information.) [b] Average of three samples. (Original mold diameter: 1.40 cm. For sample diameter before compression see Table 1.) [c] Average of three samples. [d] Single sample, average of 50 measurements. [e] By the 4 × V_{Total}/σ method. For the first number, V_{Total} was calculated by the single-point adsorption method; for the number in brackets V_{Total} was calculated via $V_{Total} = (1/\rho_b) - (1/\rho_s)$.

cryogenic temperatures. A room-temperature stress−strain curve under repetitive loading−unloading conditions is also included (red line). The inset shows a magnification of the stress−strain curve at low strains, from which we extract the Young's modulus and the compressive yield strength at 0.2% offset strain. Comprehensive data for the N3300A-derived PUA aerogels are summarized in Table 3 along with similar data from high-density X-silica and X-vanadia aerogels. Materials characterization data of fully compressed samples after testing are presented in Table 4.

At room temperature, N3300A-drived aerogels are linearly elastic only under small compressive strains (< 3%) and then exhibit plastic deformation until about 70% compressive strain, followed by densification and inelastic hardening, in pretty similar fashion to X-silica and X-vanadia aerogels. PUA samples do not buckle under compression, and they do not ultimately break into fragments, behaving in that regard similarly to X-vanadia, yielding transparent/translucent disks (above 80% strain, Figure 11) where porosity has been decreased, although has not disappeared, and almost all surface area has been lost (see Table 4). Skeletal densities are basically equal before and after compression (compare Tables 1 and 4) signifying absence of closed pores, while the wide discrepancy between average pore diameters calculated by two methods (see footnote e in Table 4) indicates that the surviving porosity is mostly due to the macropores visible by SEM (Figure 11). The Poisson's ratios (Table 3) are small within the linear elastic range (up to 5% strain) and remain small as strain increases (even up to 70% strain, Table 3). This behavior is: (a) important because low Poisson's ratios at the nonlinear region prevent the rapid increase of radial and transverse strains that are often responsible for failure of materials in compression and (b) different from that of other solid materials such as dense polymers and metals where the Poisson's ratio is relatively low (0.25−0.35) in the elastic range, but it gets quite high (near 0.5) in the plastic regime (whenever one is observed).[37] Interestingly, as further noted in Table 3, all Poisson's ratios are uniformly lower at the end of the plastic deformation regime (e.g., at 70% strain) than at the end of the elastic range (at 5% strain), indicating a mechanism change in the deformation process. Indeed, in the elastic range deformation (expansion) is due to the flexibility of the

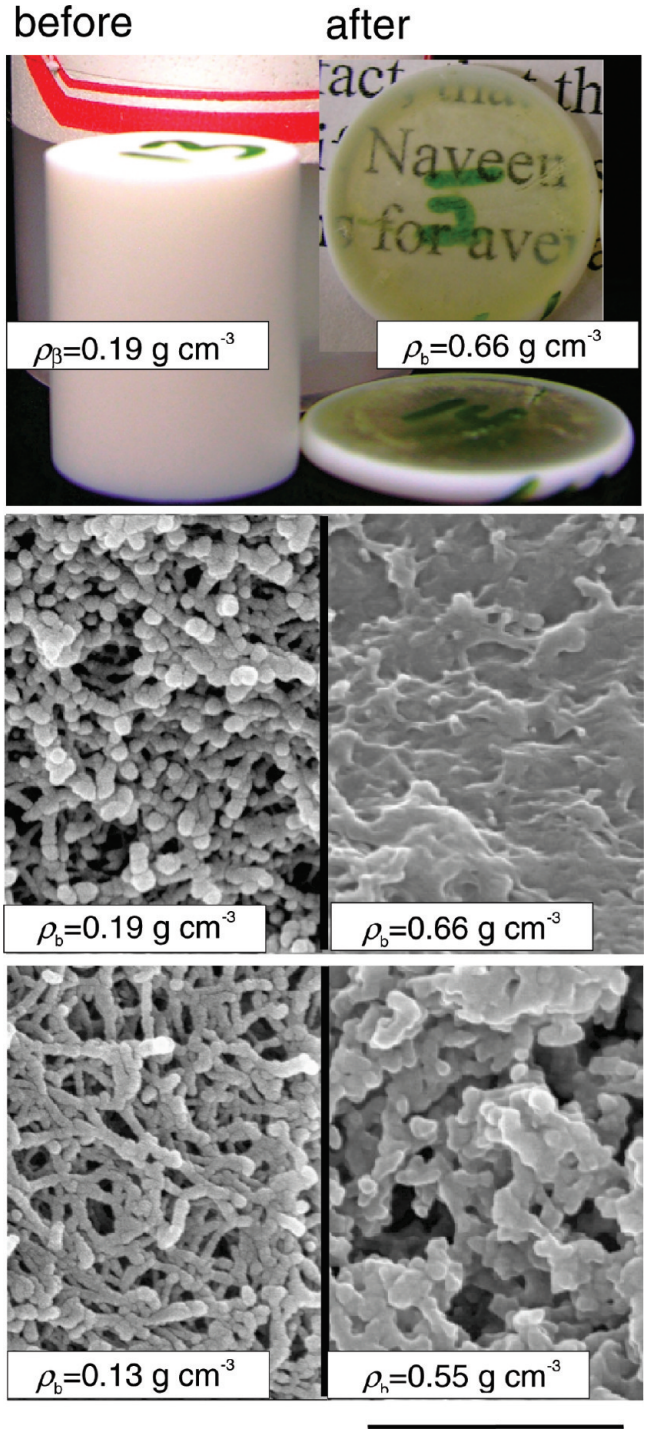

Figure 11. Optical and SEM images of a PUA aerogels before and after compression testing. Scale bar at 1 μm.

(37) Callister, W. D. *Materials Science and Engineering, An Introduction*, 7th ed.; John Wiley & Sons: New York, 2008; Appendix B.

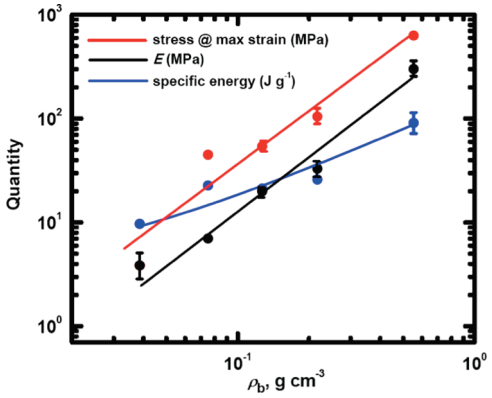

Figure 12. Log−log plot correlation of the stress at maximum strain, Young's modulus, and specific energy absorption as a function of the density of PUA aerogels derived from Desmodur N3300A triisocyanate. (Data from Table 3.)

polymer, while in the plastic regime monoliths collapse and get absorbed within their own pores. In addition, the sample micromorphology after compression (Figure 11) shows signs of melting and fusion of the skeletal nanostructures. Further, negative slopes during unloading (meaning that the material continues to contract despite the load release) and the ensuing hysteresis loops during repetitive load−unload cycles along the stress−strain curve (see Figure 10) can be also attributed to local softening and prolonged flow of the polymer for a short while even after pressure has been released. N3300A-derived polyurea melts at around 130 °C.[9] Therefore, both the direct (SEM) as well as the indirect evidence for melting (load−unload curve behavior) have to be attributed to pressure-induced sintering effects. Overall, the combination of the material being absorbed within its own porosity with softening-flow-and-retreat of the polymer within the pores reverses the natural tendency of materials to expand under compression and leads to lower Poisson ratios at higher strains.

Further insight into the mechanical behavior of the PUA aerogels can be obtained by looking more closely at the three regions of the stress−strain curve. By comparison with X-silica and X-vanadia aerogels of similar density ($\rho_b \sim 0.45-0.55$ g cm^{-3}), the elastic range of PUA aerogels is somewhat shorter, but their elastic modulus is comparable to that of the former aerogels. The shorter linear elastic range of PUA aerogels (up to 3% strain compared with 4% and 3.5% for X-silica and X-vanadia, respectively) is reflected on the lower yield strength at 0.2% offset yield strain (see Table 3). As discussed previously,[24] the elastic modulus of X-silica aerogels (see Table 3) is determined by and is practically equal to that of the underlining oxide framework (e.g., 92 ± 7 MPa for native silica at ~0.19 g cm^{-3} and 129 ± 8 MPa for X-silica at ~0.48 g cm^{-3}). On the other hand, stiffness in PUA aerogels should be controlled by the intersecondary particle (or interfiber) bridges, which are polymeric, and therefore flexible, leading to a shorter elastic range. Despite apparent changes in nanomorphology (Figure 6), the elastic modulus of N3300A-derived PUA aerogels scales exponentially with bulk density over the entire density range considered (Figure 12) obeying a power-law relationship, $E \propto (\rho_b)^a$, where $a = 1.63 \pm 0.17$. By comparison, native silica, X-silica, and X-vanadia are more sensitive to the bulk density [exponents equal to 2.59−3.53,[8b] 3.10,[24] and 1.87,[8b] respectively]. The lower density sensitivity of the Young's modulus of PUA aerogels reflects probably the more flexible nature of the exclusively polymeric framework. Finally, the Young's modulus, E, is further used for the calculation of the speed of sound, v, in PUA monoliths using $v = (E/\rho_b)^{1/2}$. Results are included in Table 3. The values for the lower density samples are as low as the speed of sound in open dry air at 20 °C (343 m s^{-1}), increasing to just over double that value in the most-dense PUA samples of this study (0.55 g cm^{-3}). Therefore, it is inferred that all PUA aerogels, and particularly those with medium to lower density, are expected to be excellent acoustic attenuators.

The ultimate compressive strength, UCS, of PUA aerogels can be quite high and, as noted in Table 3, at comparable densities PUA aerogels can be as strong materials as X-silica and X-vanadia. The failure mechanism, however, is very different from that of X-silica and resembles that of X-vanadia, most probably due to the striking similarity of their fibrilar nanostructures. In X-silica, when compression reaches a compressive strain nearly equal to the porosity, all pores are nearly fully closed and necessarily the material has to expand laterally. Thus, X-silica fails into fragments as a result of high radial and circumferential strains. In the case of X-vanadia aerogels, when compression reaches a strain level near to their porosity, pores again are nearly closed and further increase in compressive strain would induce high lateral strains. However, the entangled worm-like nanostructure seems to prevent fragmentation. Instead, nanoworms are sintered together by stress-induced melting of the polymer at the points of contact between the nanoworms,[8] and what is observed macroscopically is development of only a few radial cracks at the last stages of compression. Thus, X-vanadia samples remain as single pieces and continue to carry high compressive stresses. Overall, higher density polyurea aerogels (~0.5 g cm^{-3}) fail in a manner similar to X-vanadia, while lower density samples (e.g., ≤0.2 g cm^{-3}) do not even develop radial cracks (Figure 11). Compressed disks continue to carry loads until the platens of the testing machine come in contact. In that regard, the UCS values presented in Table 3 can be considered as lower bounds for UCS. The UCS of PUA aerogels obeys a power law relationship with the bulk density, UCS $\propto (\rho_b)^b$, where $b = 1.74 \pm 0.27$. The low value of exponent "b" implies that at low densities PUA aerogels are relatively stronger materials than X-silica and X-vanadia (e.g., the corresponding exponent for X-silica is $b = 4.14$). In turn, this has an additional, even more important consequence for the energy absorption capability (toughness, T) of PUA aerogels. The latter is the figure of merit for antiballistic applications and is calculated from the integrated area underneath the stress−strain curve. At $\rho_b = 0.55$ g cm^{-3}, PUA aerogels absorb as much as 91 J g^{-1} falling between X-silica and

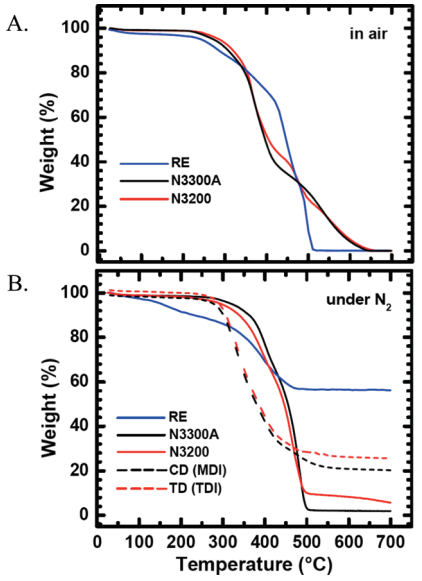

Figure 13. Thermogravimetric analysis (TGA) under N_2 of PUA aerogels derived from the isocyanates shown within the frames.

X-vanadia of similar densities (Table 3), but they far surpass materials typically considered strong such as acrylic polymers (8 J g^{-1} at 1.04 g cm^{-3}), Kevlar-49 epoxy (11 J g^{-1} at 1.04 g cm^{-3}), 4130 steel (15 J g^{-1} at 7.84 g cm^{-3}), and SiC ceramics (20 J g^{-1} at 3.02 g cm^{-3}).[38] More importantly though, the energy absorption of PUA aerogels also obeys a power low with bulk density $T \propto (\rho_b)^c$, where $c = 0.75 \pm 0.15$, meaning that PUA aerogels remain exceptionally good energy absorbers at low densities.

The effect of the fiber entanglement is particularly prevalent at cryogenic temperatures. At −173 °C, N3300A-derived aerogels become stiffer (e.g., $E = 490$ MPa at $\rho_b = 0.55$ g cm^{-3}) and more brittle, failing by fragmentation at lower strains (42−72%) than at room temperature (88−92%, Table 3). The increased stiffness is reflected on the Poisson's ratios at 5% strain, which are higher (0.30−0.33) than those observed at room temperature (0.20−0.23); but again, Poisson's ratios decrease at higher strains (0.28−0.31). The overall cryogenic behavior of PUA aerogels is intermediate between that of X-silica aerogels, which become much more brittle at those temperatures failing at just 16% compressive strain (versus 68% at room temperature), and X-vanadia aerogels, which remain ductile (Table 3). As above, those phenomena are again attributed to pressure-induced local sintering, which is given time to take effect by the entangled nanofibers of PUA and X-vanadia aerogels but not by the nanoparticulate structure of X-silica.

In summary, PUA aerogels have high strength, they are exceptional energy absorbers, and they possess high acoustic attenuation capabilities. Those properties, in combination with a facile synthesis and the expected low thermal conductivities, render those materials very attractive for several structural applications.

(38) (a) *American Society for Metals. ASM Engineering Materials Handbook, Composites*; ASM International: Materials Park, OH, 1998; Vol. *1*, p 178, Table 2. (b) Luo, H.; Chen, W. *Int. J. Appl. Ceram. Technol.* **2004**, *1*, 254–260. (c) Luo, H.; Chen, W.; Rajendran, A. M. *J. Am. Ceram. Soc.* **2006**, *89*, 266–273.

Table 5. Carbonization Data for Various PUA Aerogels upon Pyrolysis at 800 °C under Ar

PUA from:[a]	residue yield % (w/w)	C	% (w/w)[b] H	N
Desmodur N3300A	1.8			
Desmodur N3200	3.2			
Desmodur RE	56	80.72 ± 0.79	0.0	8.59 ± 0.41
Mondur CD (MDI)	19	65.42 ± 0.20	0.0	4.97 ± 0.12
Mondur TD (TDI)	25	76.66 ± 1.01	0.0	8.40 ± 0.69

[a] All samples synthesized using about 0.2 M isocyanate solutions (see Table 1) with 3.0 mol equiv of water and 0.6% (w/w) Et_3N (as defined in the Experimental Section). [b] All formulations run three times from samples from three different batches.

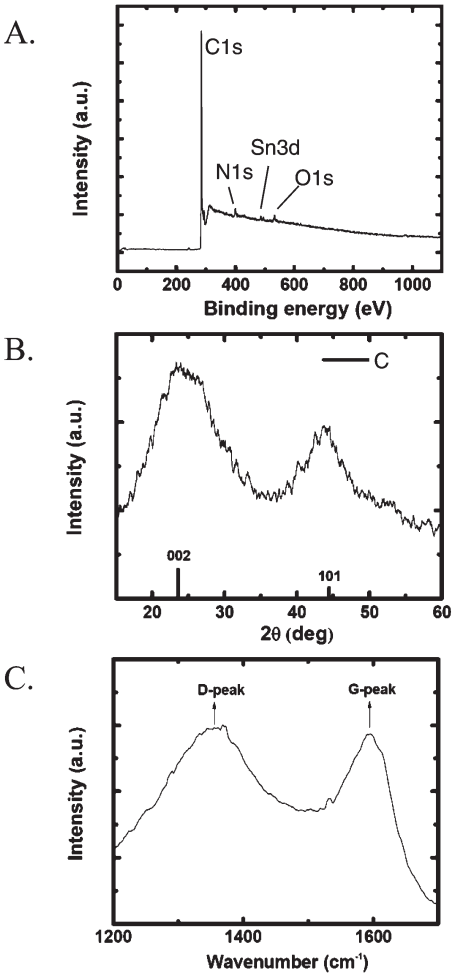

Figure 14. Representative data for carbon aerogels derived from pyrolysis of PUA aerogels ($\rho_b = 0.15$ g cm^{-3}) made from Desmodur RE aromatic triisocyanate: A. XPS (Sn comes from the sample holder). B. XRD. C. Raman spectrum.

3.3b. Pyrolytic Conversion of PUA Aerogels to Porous Carbons. Generally, carbonizable polymers are capable of either cyclizing or undergoing ring fusion and chain coalescence by heating.[39] For this, the chain should either contain aromatic moieties or be aromatizable (usually by oxidation—e.g., polyacrylonitrile). In the former case, there should be just one carbon atom between aromatic rings; otherwise, pyrolytic chain scission will prevail

(39) Jenkins, G. M.; Kawamura, K. *Polymeric Carbons, Carbon Fibre, Glass and Char*;Cambridge University Press: New York, NY, 1976.

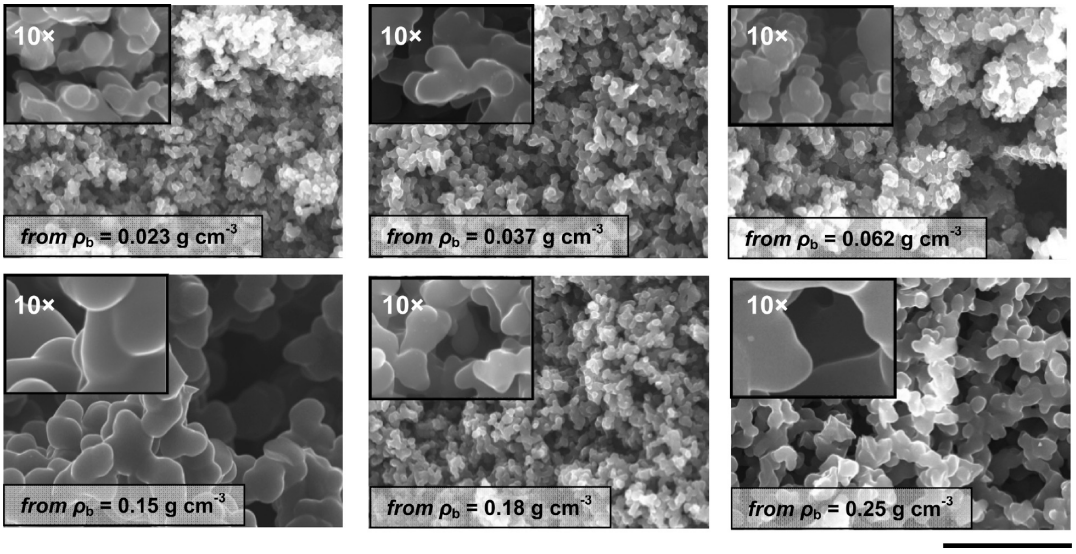

Figure 15. SEM of carbon aerogels derived from PUA aerogels made of Desmodur RE triisocyanate. Densities reported are those of the parent PUA aerogels. Scale bar: 5 μm. Morphologies should be compared with those of the PUA aerogels before pyrolysis (Figure 7). Densities of the actual C samples (from left to right): top row, not measured (sample broke to pieces); 0.29 ± 0.06 g cm^{-3}; 0.40 ± 0.02 g cm^{-3}; lower row, 0.62 ± 0.08 g cm^{-3}; 0.72 ± 0.03 g cm^{-3}; 0.78 ± 0.01 g cm^{-3}.

leading to loss of fragments.[39] Certain PUA aerogels of this study fulfill these criteria. Indeed, by TGA under N_2 (Figure 13) PUA aerogels from aliphatic isocyanates (Desmodur N3300A and N3200) decompose completely leaving only trace residues. On the other hand, PUA aerogels from aromatic isocyanates such as Desmodur RE, Mondur TD (toluene diisocyanate, TDI), and Mondur CD (4,4′-diphenylmethane diisocyanate, MDI) leave substantial amounts of residue above 500 °C. Gravimetric results after pyrolysis in a tube furnace at 800 °C under flowing Ar, along with CHN elemental analysis data, are summarized in Table 5.

The residue yield from Desmodur RE-derived aerogels is as high as that obtained from RF and polyimide aerogels.[5,40] Residues from all Desmodur RE formulations contain 78−82% (w/w) C, no H, and 5−9% (w/w) N. By XPS (Figure 14A), they also contain O in an atomic ratio to N of about equal to one. Thus, focusing on Desmodur RE-derived carbons, XRD shows very broad diffractions (Figure 14B), and typical Raman spectra (Figure 14C) show both the G (graphitic) and D (disordered) peaks at 1597 cm^{-1} and 1352 cm^{-1}, respectively, with an integrated peak intensity ratio I_D/I_G = 1.12. All data in Figure 14B,C are indicative of nanocrystalline−amorphous carbon, in agreement with skeletal density data (1.78−1.89 g cm^{-3}), which are all in the range for amorphous carbon (1.8−2.0 g cm^{-3}).[41] (Other pertinent materials characterization data are given in Table S.17 of the Supporting Information.) Looking closer to the microstructure (by SEM, Figure 15) all Desmodur RE-derived carbon samples appear macroporous and similar in appearance. The two lowest density samples have lost their string-like structure completely, although they do retain a faint memory of the wider necks observed in the 0.037 g cm^{-3} PUA samples versus those at 0.023 g cm^{-3} (compare Figures 7 and 15). The morphology of the nanoparticulate structures above 0.062 g cm^{-3} (Figure 7) is retained more closely. On the basis of those data, sintering phenomena during heating should not be ruled out, and a closer study of this type of PUA-derived carbons is certainly necessary.

4. Conclusions—Outlook

With increasing concerns over the environmental impact of the chemical industry and the unavoidable switch from a growth to a more sustainable economy, the synthesis of PUA aerogels from isocyanates and water exemplifies a more environmentally friendly approach than the classic synthesis of polyurea, because it replaces expensive amines with water. The synthesis of PUA aerogels from isocyanates and water is environmentally friendlier than the classic synthesis of polyurea as it avoids use of expensive amines. The method is also quite versatile as materials properties can be tuned conveniently and effectively by varying the chemical identity of the isocyanate among several commercially available di- and triisocyanates, aromatic versus aliphatic.

The implications of the variable nanomorphology from fibrous to particulate, by merely varying the concentration of a single reagent (the isocyanate), cannot be overemphasized. All those nanostructures consist of primary particles assembling together to form mass-fractal secondary aggregates, which in turn assemble to yet larger (mass or surface) fractal agglomerates that include fibers. Those results, considered together with our recent findings with polyimide aerogels, whereas chemically identical particles or fibers all consist of same-size primary particles,[40] seem to have fundamental significance and raise the question regarding the driving force that under certain conditions directs assembly of particles into fibers rather than globular agglomerations.

(40) Chidambareswarapattar, C.; Larimore, Z.; Sotiriou-Leventis, C.; Mang, J. T.; Leventis, N. *J. Mater. Chem.* **2010**, *20*, 9666–9678.
(41) McKenzie, D. R.; Muller, D.; Pailthorpe, B. A. *Phys. Rev. Lett.* **1991**, *67*, 773–776.

Formation of primary particles is rationalized by phase separation of an insoluble polymer. However, being able to control their assembly into fibers seems to have practical significance. Consistently with previous results obtained with inorganic fibers (e.g., vanadia) coated with polymer, the macroscopic result of entanglement is to keep the material together (via the bird-nest effect) allowing for sintering phenomena to take place, thus increasing the ultimate strain under compression and depressing the ductile-to-brittle transition upon cooling. Both effects cause an increase of the specific energy absorption of PUA aerogels into regimes unattainable even by materials that are typically considered strong (e.g., Kevlar-49 epoxy, 4130 steel, and SiC ceramics).

Finally, the importance of the high yield conversion of Desmodur RE-derived PUA aerogels into carbon is also multifaceted. Apart from the obvious implications in the context of the search for efficient methods to porous carbons, if that conversion is looked at from the perspective of the polymer-cross-linked aerogels, it can easily be seen how it may lead to new materials. For instance, recently, polyacrylonitrile (PAN)-coated silica was converted to highly porous (70% v/v) monolithic silicon carbide (SiC) aerogels.[42] That process required (a) use of a bidentate surface-confined free radical initiator and (b) aromatization of the PAN coating before carbonization and carbothermal reaction with silica. Thus far, that method has worked well with silica but cannot be extended easily to other oxide aerogels. On the other hand, polyurea cross-linking is a "genetic" approach that has been demonstrated with several nonsilica aerogels.[7d,8,43] Hence, Desmodur RE-cross-linked aerogels are directly convertible to a variety of porous metals and ceramics (carbides) according to carbothermal methods demonstrated recently with interpenetrating metal oxide/RF aerogel networks.[44]

Acknowledgment. For financial support we thank the National Science Foundation under Agreement Nos. CHE-0809562 (N.L., C.S.-L.), DMR-0907291 (N.L., H.L.), CMMI-0653970 (N.L., C.S.-L.), and CMMI-0653919 (H.L.) and the Army Research Office under Award No. W911NF-10-1-0476 (N.L., C.S.-L.). We also acknowledge the Materials Research Center of Missouri S&T for support in sample characterization (SEM, XRD). Solids NMR work was conducted at the University of Missouri Columbia by Dr. Wei Wycoff. This work benefited tremendously from the use of the SANS instrument, LQD at the Manuel Lujan, Jr. Neutron Scattering Center of the Los Alamos National Laboratory, supported by the DOE office of Basic Energy Sciences and utilized facilities supported in part by the National Science Foundation under Agreement No. DMR-0454672. We also acknowledge the support of the National Institute of Standards and Technology, U.S. Department of Commerce, in providing additional neutron research facilities used in this work. Finally, we thank Bayer Corporation USA for their generous supply of isocyanates.

Supporting Information Available: Formulations and gelation times of all samples using Desmodur N3300A, Desmodur N3200, Desmodur RE, and Mondur TD (Tables S.1−S.9); comparison of PUA xerogels, aerogels, and samples dried under ambient pressure from pentane (Table S.10); detailed data for all formulations of water and catalyst for all PUA samples prepared with Desmodur N3300A triisocyanate (Tables S.11−S.16); characterization data for carbon aerogels from Desmodur RE Aerogels (Table S.17); spectroscopic characterization data for Desmodur N3300A, Desmodur RE and Desmodur N3200 (Figures S.1−S.3); additional ^{13}C NMR data (Figures S.4−S.6); SEM of Desmodur N3300A-derived PUA aerogels as a function of H_2O and Et_3N concentration (Figure S.7). This information is available free of charge via the Internet at http://pubs.acs.org.

(42) Leventis, N.; Sadekar, A.; Chandrasekaran, N.; Sotiriou-Leventis, C. *Chem. Mater.* **2010**, *22*, 2790–2803.
(43) Leventis, N.; Vassilaras, P.; Fabrizio, E. F.; Dass, A. *J. Mater. Chem.* **2007**, *17*, 1502–1508.
(44) (a) Leventis, N.; Chandrasekaran, N.; Sadekar, A. G.; Mulik, S.; Sotiriou-Leventis, C. *J. Mater. Chem.* **2010**, *20*, 7456–7471. (b) Leventis, N.; Chandrasekaran, N.; Sadekar, A. G.; Sotiriou-Leventis, C.; Lu, H. *J. Am. Chem. Soc.* **2009**, *131*, 4576–4577. (c) Leventis, N.; Chandrasekaran, N.; Sotiriou-Leventis, C.; Mumtaz, A. *J. Mater. Chem.* **2009**, *19*, 63–65.